Loss of antibunching

Juan Camilo López Carreño [1,2] Eduardo Zubizarreta Casalengua [1] Blanca Silva [3]
Elena del Valle [1,3] and Fabrice P. Laussy [1,4]

[1]*Faculty of Science and Engineering, University of Wolverhampton, Wulfruna Street, Wolverhampton WV1 1LY, United Kingdom*
[2]*Institute of Theoretical Physics, University of Warsaw, Ulica Pasteura 5, 02-093 Warsaw, Poland*
[3]*Departamento de Física Teórica de la Materia Condensada, Universidad Autónoma de Madrid, 28049 Madrid, Spain*
[4]*Russian Quantum Center, Novaya 100, 143025 Skolkovo, Moscow Region, Russia*

We describe some of the main external mechanisms that lead to a loss of antibunching, i.e., that spoil the character of a given quantum light to deliver its photons separated from each other. Namely, we consider contamination by noise, a time jitter in the photon detection, and the effect of frequency filtering (or detection with finite bandwidth). The formalism to describe time jitter is derived and connected to the already existing one for frequency filtering. The emission from a two-level system under both incoherent and coherent driving is taken as a particular case of special interest. The coherent case is further separated into its vanishing- (Heitler) and high- (Mollow) driving regimes. We provide analytical solutions which, in the case of filtering, reveal an unsuspected structure in the transitions from perfect antibunching to thermal (incoherent case) or uncorrelated (coherent case) emission. The experimental observations of these basic and fundamental transitions would provide additional compelling evidence of the correctness and importance of the theory of frequency-resolved photon correlations.

I. INTRODUCTION

Antibunching [1] describes one of the most popular types of quantum light, the one in which photons get separated from each other and avoid the opposite bunching tendency of bosons to appear clumped together [2]. With its observation by Kimble [3], antibunching provided the first direct evidence of quantization of the light field, that is to say, the first observation, albeit indirect, of photons. Antibunched light is also of considerable importance for quantum applications, for instance, to feed quantum gates or for the already commercialized quantum cryptography, in which case one seeks the ultimate antibunching where transform-limited photons [4] are never detected more than one at a time. This is an asymptotic race, however, as perfect antibunching has still not been achieved and some residual multiple-photon emission has always accompanied the most crafted setups. In principle, since we are dealing with a quantized property, with a gap separating one value (one photon) from its neighbors (vacuum or two photons), there is no *a priori* reason why one could not observe perfect antibunching, just as one observes perfect conductivity from a superconductor or perfect flow from a superfluid. In all these cases, there are experimental limitations, inaccuracy of measurements, and finite times and energy involved, yet one can show that the measurement of resistance is compatible with a mathematical zero in a superconductor, where experiments with superconducting coils have demonstrated current flow persisting for years without degradation. This points to a lifetime for the persistent current of at least 100 000 years and with theoretical estimates to exceed the lifetime of the universe [5]. This is in this sense

that one can speak of the resistance becoming "truly zero" in a superconductor. Instead, when it comes to the more basic problem of detecting a single photon, one finds instead two-photon antibunching deviating from uncorrelated light by at best 7.5×10^{-5} [6] and 9.5×10^{-5} [7], which are furthermore sensibly better than most values reported in the ample literature (which cannot be browsed completely even if we narrow it down to recent reports below 10^{-2} [6–20]; see Ref. [21] for a recent review). The record-value antibunching [6,7] has been significantly improved by counteracting reexcitations of a two-level system (2LS) by implementing two-photon excitation schemes (in Ref. [22] we also discussed how exciting a 2LS with quantum light improves its single-photon characteristics). However, even with this newly added trick to suppress multiphoton emission, the perfect antibunching of an exact zero (or no coincidence at all regardless of the time the experiment is run) is still out of reach. In this paper we discuss mechanisms that lead to a loss of antibunching, regardless of the source of light itself, which can indeed be perfectly antibunched. We cover both technical (noise and time jitter) and more fundamental reasons (linked to photon detection).

II. DEFINITION OF ANTIBUNCHING

The definition of antibunching requires some discussion, as it varies throughout times and authors [23] and is commonly mixed with another one (sub-Poissonian statistics). At the heart of every definition, one finds Glauber's theory of optical coherence [24], which introduces correlation functions $g_a^{(n)}$ for

the nth-order coherence as

$$
g_a^{(n)}(t_1, \ldots, t_n) \\
\equiv \frac{\langle a^\dagger(t_1) a^\dagger(t_2) \cdots a^\dagger(t_n) a(t_n) \cdots a(t_2) a(t_1) \rangle}{\langle a^\dagger(t_1) a(t_1) \rangle \langle a^\dagger(t_2) a(t_2) \rangle \cdots \langle a^\dagger(t_n) a(t_n) \rangle} \quad (1)
$$

for a single mode with annihilation operator a, which is the best way to root our discussion at its most fundamental level, as involving a continuum from the start should eventually lead us to the same results. Usually, this operator a is bosonic as it refers to the photons emitted by the system. From the input-output formalism, one can however extend the definition of Eq. (1) to the field operators of the source itself, which will be the case in this paper where we study the 2LS, in which case one replaces a by the corresponding annihilation operator σ. The times t_k are in increasing order, i.e., $t_1 < t_2 < \cdots < t_n$. At the two-photon level, which is of more common occurrence, Eq. (1) reads

$$
g_a^{(2)}(t_1, t_2) = \frac{\langle a^\dagger(t_1) a^\dagger(t_2) a(t_2) a(t_1) \rangle}{\langle (a^\dagger a)(t_1) \rangle \langle (a^\dagger a)(t_2) \rangle} \quad (2)
$$

with $t_1 < t_2$, and if dealing with a steady state, so that only the time difference $\tau \equiv t_2 - t_1$ matters,

$$
g_a^{(2)}(\tau) = \frac{\langle a^\dagger a^\dagger(\tau) a(\tau) a \rangle}{\langle a^\dagger a \rangle^2}, \quad (3)
$$

with $a \equiv a(0)$ and $\langle a^\dagger a \rangle = \langle a^\dagger(\tau) a(\tau) \rangle$ for all τ by definition of stationarity. At zero time delay $\tau = 0$, Eq. (3) further simplifies to what is the most important value,

$$
g_a^{(2)}(0) = \frac{\langle a^{\dagger 2} a^2 \rangle}{\langle a^\dagger a \rangle^2}. \quad (4)
$$

The average $\langle \cdots \rangle$ in Eqs. (1)–(3) can be understood from the ergodic hypothesis as being either over statistical ensembles of the system or in time for one in isolation (with no evolution on average when assuming a steady state but fluctuations at all times in all cases). It can be further simplified for Eq. (4) as a quantum average over a density matrix ρ to yield the two-photon coincidences $g_a^{(2)}(0)$ in terms of the probabilities $p(n) \equiv \langle n | \rho | n \rangle$ of finding n photons in the system as

$$
g_a^{(2)}(0) = \frac{\sum_{n=0}^{\infty} n(n-1) p(n)}{\left[\sum_{n=0}^{\infty} n p(n) \right]^2}. \quad (5)
$$

As such, antibunching is deeply associated with photon statistics and the two-photon probability. However, nowadays, antibunching is commonly defined by the condition [25,26]

$$
g_a^{(2)}(0) < g_a^{(2)}(\tau) : \forall \, 0 \leqslant \tau < \tau_{\max}, \quad (6)
$$

where $\tau_{\max}$ can be infinite. Since for long enough time delays photons are uncorrelated, which means, by definition, that the numerator in Eq. (3) factorizes in the form of the denominator, i.e., $\lim_{\tau \to \infty} g_a^{(2)}(\tau) = 1$, then a popular understanding of antibunching reads

$$
g_a^{(2)}(0) < 1. \quad (7)
$$

This is inaccurate at best since Eqs. (6) and (7) are logically independent, i.e., neither implies the other, although they are strongly related to each other [27]. This point has been made by Zou and Mandel [28]. A proper name for Eq. (7) is sub-Poisson light (other denominations can be found such as photon-number-squeezed light [23]). This is because in this case the photon-number fluctuations as given by Eq. (5) are indeed below those of a Poisson distribution, which implies uncorrelations or a random number of photons for a given average. On the opposite extreme, the case of exactly one photon $p(n) = \delta_{n,1}$, with no fluctuations, cancels the numerator of Eq. (5), which starts at $n = 2$, and provides the perfect antibunching

$$
g_a^{(2)}(0) = 0. \quad (8)
$$

This clearly satisfies Eq. (6). Faulty reasoning in terms of integer numbers of photons only and forgetting about their superpositions led to $g_a^{(2)}(0) < \frac{1}{2}$ as a criterion for single-photon emission [29]: The value $\frac{1}{2}$ is obtained for a two-photon state $p(n) = \delta_{n,2}$ and a smaller value would thus indicate one did not get up to two photons, hence having one. This is of course incorrect as the value should then be exactly zero. Although the exact meaning of this criterion has been given [30,31], it remains a popular one [21]. The ultimate goal for antibunching therefore remains that of Eq. (8), i.e., a strict zero, since, however close to zero, the light could still be bunched if not exactly suppressing coincidences at zero delay. Such discussions truly become important for particular, and often odd, cases such as the just-discussed bunching of sub-Poissonian light or antibunching of super-Poissonian light. In this paper we focus on the simplest case, which is also that of (today's) greatest interest, of sub-Poissonian antibunched light, so such precautions in the terminology will not be entirely necessary. By antibunching, we thus understand the tendency of emitting single photons, as is often the case in the literature anyway. Note that our formalisms and results can nevertheless be applied to all types of photon correlations (bunching, super-bunching, etc.) as we will see in the following, even if we focus presently on antibunching.

III. MEASUREMENT OF ANTIBUNCHING

The typical setup for measuring antibunching experimentally is that designed by Hanbury Brown [32] to implement an intensity interferometer following his naked-eye observation of radar correlations in the early days of its elaboration. While initially designed for interferometry in radio astronomy [33], its application to visible light was quickly understood as involving photon correlations at the single-particle level, which initially caused much controversy but was quickly confirmed experimentally [34] (the denomination of "coherent" for the beams of light in Ref. [34] predates Glauber's theory of optical coherence and refers to monochromatic thermal light). The theory of the effect by Twiss gives to the setup its famed name of Hanbury Brown–Twiss (HBT) interferometer. While designed for bunching, i.e., the natural tendency of bosons whose symmetric wave functions tend to clutter together, the same setup is apt to measure all types of photon correlations, including antibunching, as had been readily predicted [35,36]. The HBT setup consists of a beam splitter followed by two detectors in each branch which are temporally correlated. In practice, the first detector that records a click starts a time counter while the other detector stops it and a

normalized histogram of the time differences τ between the successive photons thus reconstructs the second-order coherence function $g^{(2)}$. It is also known as a photon-coincidence measurement. The critical elements that affect the quantum correlations in this setup are the detectors, which are typically avalanche photodiodes (APDs) [37]. The most frequently used detectors for low-intensity light are photomultiplier tubes, but their quantum efficiency is low (less than 50%). For this reason, APDs are used, which have an additional gain mechanism, the avalanche effect. With the APDs, a stable gain on the order of 10^2-10^3 can be achieved, which is still too low to detect single photons. For this purpose, the APDs must be used in the Geiger mode [38]. These single-photon avalanche photodiodes have a high detection efficiency and low dark count rates, but they are slow and with a big timing jitter (typically 300–400 ps, with low values of 35 ps [39]). To multiply the signal, they use semiconductor materials. Depending on these materials, the APDs can operate in different frequency windows between 550 and 1550 nm. Another source of noise characteristic of APDs is the afterpulsing, which can limit the count rate [40].

New methods have emerged to measure photon correlations, in particular one that relies on a direct observation of the photon streams as measured by a streak camera [41]. The detected photons are first transformed into photoelectrons by means of a photocathode. These new photoelectrons are deflected vertically to different pixels on the detector as a function of time. Due to this shift, the vertical position on the detector defines the time of arrival of the photon. Streak cameras have low detection efficiency but allow for a resolution of the order of picoseconds. They operate in frequency windows of 300–1700 nm, depending on the material used for the photocathode. One advantage of a streak camera setup in a cw regime is that it provides the raw result with no need for postprocessing or normalization. Namely, the condition $g^{(2)}(\tau \to \infty) = 1$, which is used to normalize the signal in the case of an HBT measurement, should be automatically fulfilled with the streak setup. Failure to be the case should indicate some problem in the detection, e.g., nonstationarity of the signal [42]. This allows as well one to compute higher-order photon correlations, which can also be achieved with other emerging techniques such as transition edge sensors set up to directly resolve the number of detected photons [43].

With this brief overview of some of the main and newest methods to measure antibunching, one gets a feeling of the mechanisms that lead to its loss and that we will model theoretically in the following. These include, basically, external noise and time uncertainty in the detection. The latter can be due to jitter, meaning fluctuation or scrambling of the arrival time due to the detector, or at a more fundamental level be linked to the time-energy uncertainty which is inherent even to ideal detectors. We will cover both mechanisms. Interestingly, photon losses, which constitute an important limitation of all schemes of photon detection, are not detrimental for the measurement of $g^{(2)}(\tau)$. This merely dims the signal, but preserves its statistics. Although only a coherent signal can pass a linear optical element without being distorted and sub-Poissonian or super-Poissonian signals get closer to Poissonian distributions, e.g., by passing through beam splitters [44], this however refers to the noise of the signal rather than

to its statistics. A well-ordered stream of single photons would appear less ordered in the presence of losses, but this would in no way lead to spurious coincidences. Such a closeness to a Poissonian distribution is typically measured by the Fano factor, which relates the width of the input distribution to the expected one for a Poissonian distribution with the same average number as $F = (\langle n^2 \rangle - \langle n \rangle^2)/\langle n \rangle$. Therefore, as the Fano factor can grow linearly from 0, corresponding to a number-state distribution, to 1, corresponding to a Poisson distribution, as the probability to lose any one photon of the input beam is increased, the statistics as measured by $g^{(2)}(0)$ remains constant, equal to that of the ideal signal. This is clear on physical grounds since removing photons to an antibunched signal cannot create bunching. What is spoiled is the signal, which can however be compensated by longer integration times. The loss is therefore in quantity, not in quality. This features makes the lossy setups, including the HBT one, able to measure antibunching [45], as it does not matter that strictly successive photons are recorded, $g^{(2)}(\tau)$ being a density probability for any two photons to be separated by the interval τ, regardless of whether other photons are present in between. In fact, a histogram of exactly successive photons would fail to produce the uncorrelated plateau at long τ. We can therefore already eliminate one of the main difficulties encountered in the experiment and focus on the other above-cited mechanisms. Before turning to them in detail, we first review the antibunching from the source we will use to illustrate the general theory, which is of great interest regardless, being the most fundamental and widespread type of single-photon source.

IV. EXAMPLES OF ANTIBUNCHING

The two-level system is the paradigmatic source of single photons. When the emission occurs with the system relaxing from its excited state to its ground state, and since it takes a finite amount of time for the 2LS to be reexcited, together with the impossibility to host more than one excitation at a time, two photons can never be emitted simultaneously. This is at least the basic picture which one can form and that applies in the simplest cases of incoherent excitation as well as strong coherent excitation. Under weak coherent excitation, on the other hand, subtle interferences at the multiphoton level also produce antibunching but with a distinct physical origin [46]. In the rest of the paper we will work with the cases of incoherent and coherent excitation, the latter being further separated into its weak- (Heitler) and high- (Mollow) driving regimes.

A. Incoherent excitation

The Hamiltonian of an incoherently driven 2LS is simply its free energy, namely,

$$H_\sigma = \omega_\sigma \sigma^\dagger \sigma, \tag{9}$$

where the 2LS is described through the annihilation operator σ, which satisfies the algebra of pseudospins, and ω_σ is the natural frequency of the 2LS. Both the excitation and decay of the 2LS are taken into account by turning to a master equation

(we use $\hbar = 1$ throughout the paper)

$$\partial_t \rho = i[\rho, H_\sigma] + \sum_k \mathcal{L}_{c_k} \rho, \qquad (10)$$

with the Lindblad terms $\mathcal{L}_{\sigma^\dagger} \rho = (P_\sigma/2)(2\sigma^\dagger \rho \sigma - \sigma \sigma^\dagger \rho - \rho \sigma \sigma^\dagger)$, where P_σ is the rate of excitation, and $\mathcal{L}_\sigma \rho = (\gamma_\sigma/2)(2\sigma \rho \sigma^\dagger - \sigma^\dagger \sigma \rho - \rho \sigma^\dagger \sigma)$, where γ_σ is the decay rate [47–49]. It is then a simple algebraic procedure to obtain the second-order correlations of a 2LS, $g_\sigma^{(2)}(\tau) = \frac{\langle \sigma^\dagger \sigma^\dagger(\tau)\sigma(\tau)\sigma \rangle}{\langle \sigma^\dagger \sigma \rangle^2}$ [cf. Eq. (3)], under incoherent pumping P_σ, as

$$g_{\sigma,P_\sigma}^{(2)}(\tau) = 1 - e^{-\Gamma_\sigma \tau}, \qquad (11)$$

in terms of the effective decay rate $\Gamma_\sigma \equiv \gamma_\sigma + P_\sigma$ that causes the power broadening of the emission spectrum.

B. Coherent excitation

The counterpart of the preceding section for coherent excitation is described by the Hamiltonian

$$H_{\Omega_\sigma} = \omega_\sigma \sigma^\dagger \sigma + \Omega_\sigma (\sigma e^{i\omega_L t} + \sigma^\dagger e^{-i\omega_L t}) \qquad (12)$$

and, subsequently, by the master equation

$$\partial_t \rho = i[\rho, H_{\Omega_\sigma}] + \frac{\gamma_\sigma}{2}(2\sigma \rho \sigma^\dagger - \sigma^\dagger \sigma \rho - \rho \sigma^\dagger \sigma), \qquad (13)$$

where Ω_σ^2 is the intensity at which the 2LS is driven by a laser of frequency ω_L. The temporal dependence in Eq. (12) is removed by making a Dirac transformation, leaving the contribution from the free energy of the 2LS [Eq. (9)] proportional to the *detuning* $\Delta_\sigma \equiv \omega_\sigma - \omega_L$ between the laser and the 2LS's natural frequencies. We will focus on the strict "resonance" of resonance fluorescence, meaning $\Delta_\sigma = 0$ (the emitter is driven at the frequency at which it emits). The same techniques applied to this variation of the problem provide the correlations for the 2LS under coherent excitation as

$$g_{\sigma,\Omega_\sigma}^{(2)}(\tau) = 1 - e^{-3\gamma_\sigma \tau/4}\left[\cosh\left(\frac{\gamma_M \tau}{4}\right) + \frac{3\gamma_\sigma}{\gamma_M}\sinh\left(\frac{\gamma_M \tau}{4}\right)\right], \qquad (14)$$

where $\gamma_M \equiv \sqrt{\gamma_\sigma^2 - (8\Omega_\sigma)^2}$ (M is for Mollow). This more involved expression accounts for both regimes of low and high driving. In the Heitler regime [50], where the rate of excitation is much weaker than the decay rate of the 2LS, the correlations simplify to

$$g_{\sigma,\Omega_\sigma \to 0}^{(2)}(\tau) = (1 - e^{-\gamma_\sigma \tau/2})^2, \qquad (15)$$

and in the limit of large driving, the correlations are strongly oscillating (with frequency $2\Omega_\sigma$) between the envelopes

$$g_{\sigma,\Omega_\sigma \to \infty}^{(2)}(\tau) = 1 \pm e^{-3\gamma_\sigma \tau/4} \qquad (16)$$

that decay from 0 and 2, respectively, to 1. All the expressions in Eqs. (11) and (14)–(16) are autocorrelations and as such they are symmetric functions, namely, $g_\sigma^{(2)}(-\tau) = g_\sigma^{(2)}(\tau)$.

Already, we have more than enough material to study from this basic emitter the highly nontrivial physics of loss of antibunching, and we will focus the rest of our discussion on this case. Other antibunched sources would either behave similarly and/or could be studied following a similar approach.

V. LOSS OF ANTIBUNCHING BY NOISE CONTAMINATION

A first obvious and simple way that antibunching can be lost is due to the signal being perturbed by noise. Dark counts, for instance, which correspond to photon detection even in the absence of light (whence the name) [51], clearly spoil antibunching, since the extra photon can arrive simultaneously with a signal photon that was supposed to be detected in isolation. Also, in some cases, the laser driving the system can directly inject a spurious fraction of photons into the detectors [52]. All these photons that are uncorrelated with the source cause a random noise, or shot noise, which (usually) spoils antibunching (shot noise usually assumes Poissonian statistics of the noise).

If we call $I(t)$ the instantaneous photon intensity from the source (signal) and $I'(t)$ that of the randomly added photons (noise), the total final intensity is given by

$$I^*(t) = I'(t) + I(t) \qquad (17)$$

and the photon statistics of the total signal is given by

$$g^{*(2)}(t, \tau) = \frac{\langle :I^*(t)I^*(t + \tau): \rangle}{\langle I^*(t) \rangle^2}, \qquad (18)$$

where $:\cdots:$ normally orders the operators so that they appear in the form of Eq. (2), without which the Cauchy-Schwarz inequality forbids antibunching [in the form of Eq. (6)]. Since the signal and noise are uncorrelated $\langle :I(t)I'(t'): \rangle = \langle I(t) \rangle \langle I'(t') \rangle$ for all t, t', and with ξ, the noise-to-signal ratio, i.e., $\xi(t) \equiv \langle I'(t) \rangle / \langle I(t) \rangle$, one can get a simple expression that relates the photon statistics of the signal contaminated by the noise with statistics $g'^{(2)}(\tau) \equiv \langle :I'(t)I'(t + \tau): \rangle / \langle I'(t) \rangle^2$ to that of the original signal $g^{(2)}(\tau)$ as

$$g^{*(2)}(t, \tau) = \frac{g^{(2)}(t, \tau) + \xi(t)\xi(t+\tau)g'^{(2)}(\tau) + \xi(t) + \xi(t + \tau)}{(1 + \xi)^2}. \qquad (19)$$

This is straightforwardly applied to the case of a stationary signal, in which case Eq. (19) becomes $g^{*(2)}(\tau) = [g^{(2)}(\tau) + \xi^2 g'^{(2)}(\tau) + 2\xi]/(1 + \xi)^2$, where ξ is now a constant. If the noise has no correlation, $g'^{(2)}(\tau) = 1$ for all τ, and for perfect antibunching with $g^{(2)}(0) = 0$, the loss of antibunching $\xi(2 + \xi)/(1 + \xi)^2$ requires a noise-to-signal ratio of $\sqrt{2} - 1 \approx 42\%$ to spoil it to 0.5; even when there is twice as much noise as perfectly antibunched signal, the resulting antibunching of $\frac{8}{9} \approx 0.89$ is still clearly observed. The random noise tends to flatten the correlations to that of an uncorrelated (coherent) signal with $g^{*(2)}(\tau) = 1$ everywhere, in a way that shifts the curves to one, without transforming bunching into antibunching or vice versa [53]. It also has no effect on the coherence time (the time necessary for the correlation to converge to one is independent of the percentage of noise). Thermal noise, not surprisingly, is more detrimental to antibunching, with $\xi = \frac{1}{3}$ to spoil perfect antibunching to 0.5, and when the noise and signal are equal in intensity, then $g^{*(2)}(0) = 1$, with super-Poissonian statistics for higher ξ. Depending on the coherence time of the thermal light, $g^{*(2)}(\tau)$ is either bunched or antibunched in the sense of decreasing or increasing correlations in time. If the noise itself is antibunched, it cannot increase $g^{*(2)}(0)$ beyond 0.5, which it does when $\xi = 1$. Further noise reduces $g^{*(2)}(0)$ again as the original signal becomes the noise

for the now dominating antibunching. In all cases, in the limit $\xi \to \infty$, $g^{*(2)}(\tau) \to g'^{(2)}(\tau)$ and then one observes the noise itself, so what is lost is indeed the antibunching of the signal (such as its coherence time). Finally, we commented already how a possible source of noise is from the driving laser itself. We have assumed in this discussion that the noise and signal are independent and do not interfere, so their intensity is simply added in a way reminiscent of a classical picture of photons as particles which are superimposed onto others. In this respect, the normal ordering above plays no direct role and one could understand the result with classical stochastic fields I which are not number operators. In contrast, it could also be the case that the admixing of the two quantum fields is done at the level of their amplitudes, in which case the description would need to be with quantized fields along the lines of Ref. [54] where time and operator orderings would be significant and more complex correlations could be obtained as a result.

VI. LOSS OF ANTIBUNCHING BY TIME UNCERTAINTY

We now turn to the loss of antibunching due to a time uncertainty in the detection of the photons. Such a scenario can be due to a dead time of the detector or a jitter effect. In both cases, the result is that a photon arriving at the detector at a time t_0 is reported by the latter at some other time $t_0 + t$, with t following a probability distribution $D_\Gamma^2(t)$, which we will refer to as the jitter function. The parameter Γ is the inverse of the characteristic jitter time in the sense that it is a measure of the width of the distribution. Independently of Γ, since we assume perfect detection, the jitter function must be such that

$$\int_{-\infty}^{\infty} D_\Gamma^2(t)dt = 1, \qquad (20)$$

implying that all the photons that arrive at the detector are ultimately reported. The temporal structure of the photon stream that is received by the detector is modified by the jitter function. Its effect can be formally taken into account through the physical spectrum of emission, defined as [55]

$$S_\Gamma^{(1)}(\omega, T) = \frac{1}{2\pi} \iint_{-\infty}^{\infty} D_\Gamma(T - t_1) D_\Gamma(T - t_2)$$
$$\times e^{i\omega(t_2 - t_1)} \langle \sigma^\dagger(t_1)\sigma(t_2) \rangle \, dt_1 dt_2, \qquad (21)$$

where σ is the annihilation operator of the field emitting the photons and ω and T are the frequency and time at which these photons are being emitted. While we will later on apply the theory to the case where σ describes a 2LS, the theory is general and holds for any single-mode field. Integrating Eq. (21) in frequency leads to the time-resolved population $S_\Gamma^{(1)}(T) \equiv \int_{-\infty}^{\infty} S_\Gamma^{(1)}(\omega, T)d\omega$ which, using $\int_{-\infty}^{\infty} e^{-i\omega(t_2 - t_1)}d\omega = 2\pi\delta(t_2 - t_1)$, gives

$$S_\Gamma^{(1)}(T) = \int_{-\infty}^{\infty} D_\Gamma^2(T - t)\langle \sigma^\dagger \sigma \rangle(t)dt. \qquad (22)$$

Namely, the time-resolved population of the light emitted is the convolution of the population with the jitter function. If the signal is in a steady state, then the population is independent of time, $\langle \sigma^\dagger \sigma \rangle = n_\sigma$, and we find that the time-resolved population is equal to the total intensity, $S_\Gamma(T) = n_\sigma$, and that the jitter does not play a role in this observation. This makes sense since in the steady state, shuffling the times at which the photons are reported does not change the mean number of detected photons per unit time.

Applying the same treatment to the intensity-intensity correlation function describes the effect of the time jitter on $g^{(2)}(\tau)$ which now persists even in the steady state. Instead of the physical spectrum, one starts in this case with the second-order correlation function resolved in time and frequency [56]

$$S_{\Gamma_1\Gamma_2}^{(2)}(\omega_1, T_1; \omega_2, T_2) = \frac{1}{(2\pi)^2} \iiiint_{-\infty}^{\infty} dt_1 dt_2 dt_3 dt_4 D_{\Gamma_1}(T_1 - t_1) D_{\Gamma_1}(T_1 - t_4) D_{\Gamma_2}(T_2 - t_2) D_{\Gamma_2}(T_2 - t_3)$$
$$\times e^{i\omega_1(t_4 - t_1)} e^{i\omega_2(t_3 - t_2)} \langle \mathcal{T}_-[\sigma^\dagger(t_1)\sigma^\dagger(t_2)] \mathcal{T}_+[\sigma(t_3)\sigma(t_4)] \rangle, \qquad (23)$$

where Γ_1 and Γ_2 accommodate the fact that the pair of photons can be recorded by detectors with different jitters, $\mathcal{T}_+$ and $\mathcal{T}_-$ mean time reordering of the operators so that the first time is to the far right and the last time to the far left, respectively, and the whole expression is likewise time ordered. Assuming that the jitter for both detectors are equal (i.e., $\Gamma_1 = \Gamma_2 = \Gamma$), the frequency-integrated quantity $S_\Gamma^{(2)}(T_1; T_2) = \iint_{-\infty}^{\infty} S_{\Gamma_1\Gamma_2}^{(2)}(\omega_1, T_1; \omega_2, T_2)d\omega_1 d\omega_2$ becomes

$$S_\Gamma^{(2)}(T_1; T_2) = \iint_{-\infty}^{\infty} D_\Gamma^2(T_1 - t_1) D_\Gamma^2(T_2 - t_2)$$
$$\times \langle \mathcal{T}_-[\sigma^\dagger(t_1)\sigma^\dagger(t_2)] \mathcal{T}_+[\sigma(t_2)\sigma(t_1)] \rangle \, dt_1 dt_2, \qquad (24)$$

which corresponds to the intensity correlations between two branches of a split signal that is affected by the same time

jitter. Time ordering of the operators leads to two integration regions $t_1 > t_2$ and $t_2 > t_1$, which allows us to express Eq. (24) in terms of the standard $G^{(2)}(t, \Delta t) = \langle a^\dagger(t)a^\dagger(t + \Delta t)a(t + \Delta t)a(t) \rangle$ of the system, setting $t = \min(t_1, t_2)$ and $\Delta t = |t_1 - t_2|$,

$$S_\Gamma^{(2)}(T_1; T_2)$$
$$= \int_{-\infty}^{\infty} dt \int_0^{\infty} d\Delta t \, G^{(2)}(t, \Delta t)[D_\Gamma^2(T_1 - t)D_\Gamma^2(T_2 - t - \Delta t)$$
$$+ D_\Gamma^2(T_1 - t - \Delta t)D_\Gamma^2(T_2 - t)], \qquad (25)$$

where $0 \leqslant \Delta t < \infty$ represents the delay between the two detected photons. The second-order correlations function of the stream of photons affected by the time jitter is then obtained by normalizing Eq. (25) with Eq. (22) as

$$g_\Gamma^{(2)}(T_1; T_2) = S_\Gamma^{(2)}(T_1; T_2)/[S_\Gamma^{(1)}(T_1)S_\Gamma^{(1)}(T_2)]. \qquad (26)$$

In the case of a steady state, it is convenient to express the correlations as a function of the time delay between the photon pairs (the initial time is irrelevant in this case). This provides the main result of this section in the form of the jittered $g_\Gamma^{(2)}$ expression from that of the original signal as affected by the jitter function D_Γ,

$$g_\Gamma^{(2)}(\tau) = \int_0^\infty g^{(2)}(\theta) \int_{-\infty}^\infty \left[D_\Gamma^2(-t-\theta) D_\Gamma^2(\tau-t) \right.$$
$$\left. + D_\Gamma^2(-t) D_\Gamma^2(\tau-t-\theta) dt \right] d\theta, \qquad (27)$$

where we have used the fact that in the steady state $S_\Gamma^{(1)}(T) = n_\sigma$ is independent of time and $g^{(2)}(\theta)$ is the second-order correlation of the photon stream *without* the time jitter. Equation (27) is general: It holds for any $g^{(2)}(\theta)$ (as long as it is obtained in the steady state). It shows that the correlations with time jitter are obtained by weighting the original correlation function with a quantity that depends only on the jitter function. We now consider a few particular cases, describing a possible physical origin for each of them. The analytical expressions for the corresponding photon correlations for the emission from a two-level system in the various regimes of excitation, applied to the textbook expressions (11) and (14), can be obtained in all theses cases, but they are bulky and not enlightening *per se*; therefore we provide their full expression in the Appendixes. All the distributions have been chosen such that their variances are identical, namely, equal to $1/\Gamma^2$, so as to compare them usefully (the variance is a better indicator of the effect of the distribution on antibunching than the mean).

(i) The Heaviside function describes a device that has no time resolution within a given time window, in which case the jitter function reads

$$D_\Gamma(t) \equiv \sqrt{\frac{\Gamma}{\sqrt{12}}} \theta\left(1 - \frac{2\Gamma t}{\sqrt{12}}\right) \theta\left(1 + \frac{2\Gamma t}{\sqrt{12}}\right), \qquad (28)$$

where $\theta(t)$ is the Heaviside function and the distribution in Eq. (28) is only nonzero in the interval $|t| < \sqrt{3}/\Gamma$ (chosen again so that the variance of the jitter is $1/\Gamma^2$), as shown in Fig. 1(i). This could correspond to a streak camera which randomizes the time information within one pixel of the CCD camera [57]. The filtered correlations are given by Eq. (A2) for incoherent excitation and by Eq. (A3) for coherent excitation.

(ii) The exponential function describes a device that is equally likely to trigger the signal at any moment that follows its excitation, with the jitter function

$$D_\Gamma(t) = \sqrt{\Gamma} \theta(t) e^{-\Gamma t/2}, \qquad (29)$$

where $\theta(t)$ is the Heaviside function, as shown in Fig. 1(ii). This describes a wide class of devices with a memoryless dead time. The filtered correlations are given by Eq. (A5) for incoherent excitation and by Eq. (A6) for coherent excitation.

(iii) The double-exponential function, also known as the Laplace distribution, describes a device that has a memoryless dead time not only in its signal emission, like the previous type, but also in its excitation time, with the jitter function

$$D_\Gamma(t) = \sqrt{\frac{\Gamma}{\sqrt{2}}} e^{-|t|\Gamma/\sqrt{2}}, \qquad (30)$$
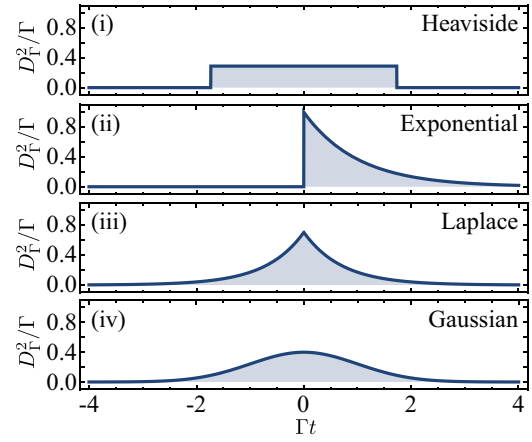
FIG. 1. Jitter functions considered in this text, namely, (a) Heaviside (28), (b) single exponential (29), (c) double exponential (Laplace) (30), and (d) Gaussian, (31), all with the variance $1/\Gamma^2$. A photon from the original signal at time 0 is replaced by one at time t following the respective distributions.

as shown in Fig. 1(iii). It can be seen as a refinement of the two previous cases, where the variation at which the photons are reported can be both delayed and advanced according to an exponential function. The filtered correlations are given by Eq. (A9) for incoherent excitation and by Eq. (A10) for coherent excitation.

(iv) Finally, the Gaussian function describes normally distributed fluctuations in the detection time, with the jitter function

$$D_\Gamma(t) = \frac{\sqrt{\Gamma}}{(2\pi)^{1/4}} e^{-(\Gamma t/2)^2}, \qquad (31)$$

as shown in Fig. 1(iv). This could be due to, e.g., the electronics involved in the detection of a photon after its arrival or various types of noise [58]. The filtered correlations are given by Eq. (A13) for incoherent excitation and by Eq. (A14) for coherent excitation.

The two-photon correlations as seen by a detector with the four types of time jitters just described are shown in Fig. 2 for incoherent excitation and in Fig. 3 for coherent excitation, as follows from the analytical expressions given in the Appendixes. The most striking result is that while various types of jitter result in an overall identical loss of antibunching, the robustness of the photon correlations depends on the type and the regime of driving, even though the emitter is the same (2LS). Specifically, the most robust photon correlations are from the coherent driving in the Heitler regime. This can be understood from the coherence time of the Heitler correlations, being larger than for the others. Comparing Figs. 2(c) and 3(c) (the traces of the former are reproduced in light gray in the latter), one can see how the Mollow regime, the incoherent 2LS, and finally the Heitler regime appear in order of least robust to most robust (the same amount of any type of jitter affects much more the Mollow antibunching than it does its Heitler counterpart). This comparison is direct for the vanishing drivings $P_\sigma \to 0$ and $\Omega_\sigma \to 0$ as it allows us to superimpose both graphs with the same axes. For small enough jitter ($\gamma_\sigma/\Gamma \lesssim 0.1$ in the figure), the Mollow antibunching
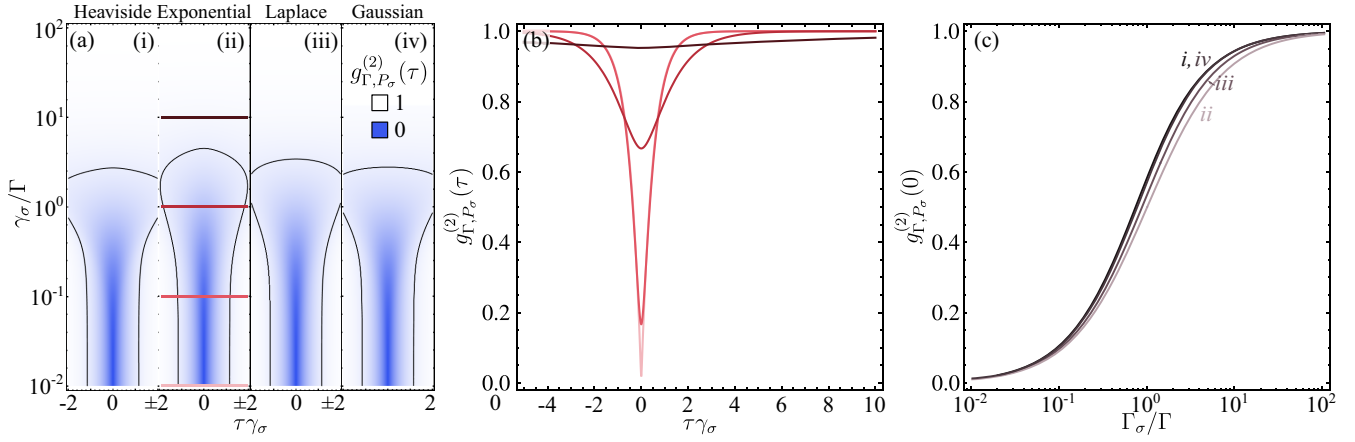
FIG. 2. Photon correlations with various types of time jitter for the incoherently driven 2LS. (a) Transition from perfect antibunching when the jitter vanishes (corresponding to a large Γ of the jitter functions) to uncorrelation when jitter is large. The progression occurs at different speeds depending on the type of jitter, namely, (i) Heaviside, (ii) single exponential, (iii) double exponential (Laplace), and (iv) Gaussian. The black contours shows the isolines $g^{(2)}_{\Gamma,P_\sigma} = 0.9$. (b) Cuts along the lines marked in (a ii) (single exponential). (c) Zero-delay correlations for the various types of jitter, which only cause small quantitative departures that are not even discernible for cases (i) and (iv).

actually gets more robust than the incoherent 2LS, which is itself more sensitive to time shifts than the Heitler case. The antibunching in this limit of small values of the x axes for the various types of jitters is

$$g^{(2)}_{\Gamma,P_\sigma}(0) = C_j \frac{\Gamma_\sigma}{\Gamma}, \tag{32a}$$

$$g^{(2),\text{Heitler}}_{\Gamma,\Omega_\sigma}(0) = \frac{\gamma_\sigma^2}{2\Gamma^2}, \tag{32b}$$

with C_j a coefficient that corresponds to the jitter types listed in Fig. 1 for $j = $ i, ii, iii, iv, which one can obtain from the

expressions given in Appendix A as $C_\text{i} = 2\sqrt{3}/3$, $C_\text{ii} = 1$, $C_\text{iii} = 3\sqrt{2}/4$, and $C_\text{iv} = 2/\sqrt{\pi}$. In the coherent case, the Heitler regime has the same limiting case for all types of jitters, while the Mollow regime is a complicated function of the parameters Ω_σ, γ_σ, and Γ, which we do not provide but that differ for the various types of jitter. The $\gamma_\sigma \to 0$ limit converges to nonzero values of $g^{(2)}_{\Gamma,\Omega_\sigma}(0)$ for finite jitter in both the incoherent and Mollow cases. In the incoherent case, this indeed plateaus to $C_j \gamma_\sigma / \Gamma$. The Heitler case and the Gaussian jitter in the Mollow case both go to zero to leading order. The other Mollow cases plateau to complicated functions of
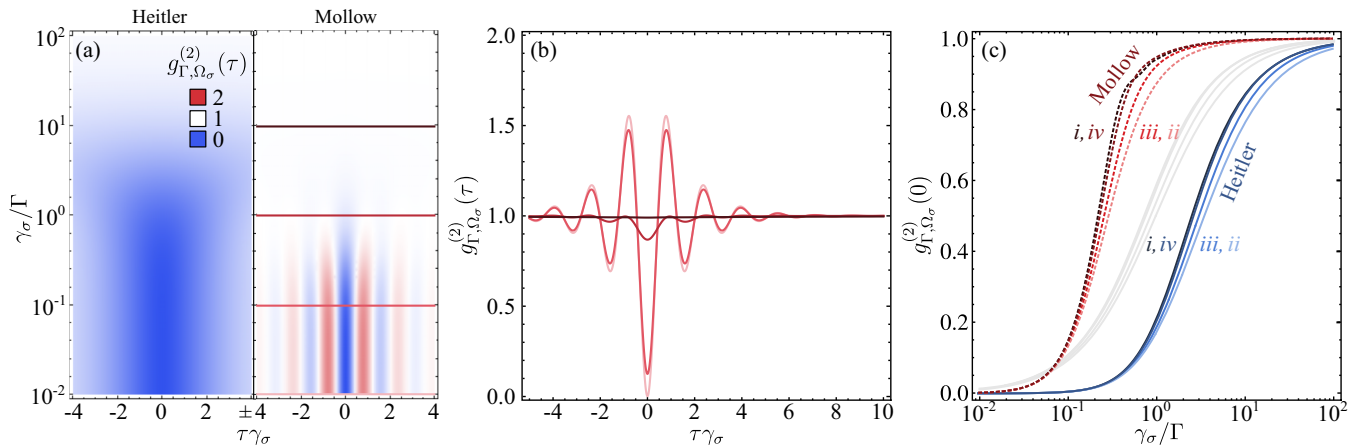
FIG. 3. Photon correlations with various types of time jitter for the coherently driven 2LS. (a) The loss of antibunching depends strongly on the regime of excitation, i.e., in the Heitler regime (left) the transition to uncorrelation requires a greater time jitter than in the Mollow triplet regime (right). The behavior with the four jitter functions follows the trend shown in Fig. 2(a) and therefore we only show the case for the single exponential. (b) Cuts along the lines marked in (a) for the Mollow triplet, showing the dampening of the correlations as the jitter increases. (c) Zero-delay correlations. The blue solid and red dashed lines correspond to the 2LS driven in the Heitler and Mollow regimes, respectively. The Heitler regime depends only on γ_σ / Γ, so the plot covers all cases (of sufficiently small driving). The Mollow regime also depends on Ω_σ which is here taken as $2\gamma_\sigma$. Higher values of Ω_σ further shift the family of curves to the left. The various lines i–iv correspond to the different jitter functions, namely, Heaviside, double exponential, single exponential, and Gaussian, respectively. The incoherent-case counterparts from Fig. 2(c) for the corresponding case of vanishing driving $P_\sigma \to 0$ are also shown in light gray for comparison. While the type of jitter bears little impact on the loss of antibunching, both the type of driving and its regime have a considerable influence.

the parameters, which is not necessary to provide explicitly. All go to zero as $\Gamma \to \infty$ (no jitter). Such limiting cases are interesting to compare the loss of antibunching between the various types and regimes of driving. It is well known that resonant excitation yields stronger antibunching, but this is attributed to the cleaner environment that is free of carriers, heating, etc. Here we find that at a fundamental level too, resonant excitation typically produces a stronger antibunching in the sense that it is more resilient to factors that spoil it.

The Heaviside and Gaussian types of jitter lead to almost identical losses of antibunching, suggesting that spreading more photons (these two distribution are flatter) has a worse effect than displacing fewer of them but farther. There is nevertheless a difference between the Heaviside and Gaussian types of jitter in the Mollow case, since the former shifts photons from the time window where $g^{(2)}(\tau) < 1$ to that where it is greater than 1 "all of a sudden" as a function of Γ, while the Gaussian type perceives the $g^{(2)}(\tau) > 1$ region in advance. The same happens for a still larger Γ now returning to a region where $g^{(2)}(\tau) < 1$. These successions lead to ripples in the loss of antibunching with the Heaviside type of jitter. This is a small, but qualitative, departure between the two types of jitter. In all cases, the single-exponential memoryless jitter is the one that least affects the antibunching. Since the exact quantitative results differ only slightly from one type of jitter to the other, we show the traces for the loss of antibunching for one case only (ii, single exponential) in Figs. 2(b) and 3(b), where the temporal dependence also exhibits a change in the correlation time in addition to the damping of the correlations. In all cases, in the limit of large widths of the jitter noise, the correlations follow a Poisson distribution. The mean uncertainty of the times at which the photons are observed increases to a point where times are essentially randomized. While this is true regardless of the type of jitter, the speed of this randomization varies.

As a concluding remark, it would be interesting for practical purposes to tackle the reverse problem of deconvoluting Eq. (27) so as to obtain the original $g^{(2)}(\theta)$ from the measured $g_\Gamma^{(2)}(\tau)$ in the presence of time jitter. In cases where the main cause of the loss of antibunching is due to such a mechanism, that would allow us to get a more faithful characterization of the source regardless of secondary issues from the surrounding equipment. Such attempts are furthermore commonplace in the literature [29,59–79], although how legitimate and accurate the recovery procedure is in all cases is still unclear to us, since it applies only for this particular type of antibunching loss (it could be, for instance, quite meaningless for that discussed in the next section) and through a procedure that appears to be oversimplified in view of the general expression given above.

VII. LOSS OF ANTIBUNCHING BY FREQUENCY FILTERING

Antibunching is also spoiled in another way, this time more fundamental since it is inherent to any detection process. Consider a photon counting experiment in which one has information not only about the time of arrival, but also about the frequency (or energy) of the detected photon. In such a scenario, Heisenberg's uncertainty principle applies:

A perfect resolution of the time of arrival (and therefore, in the absence of jitter, of the time of emission) results in a complete uncertainty of the frequency of the photons. Satisfying this condition allows one to observe the perfect antibunching of the source if it is there, as is the case with a 2LS, for which the second-order correlation functions, given in Eq. (11) for incoherent driving and in Eq. (14) for coherent driving, is exactly zero at $\tau = 0$. However, gaining information about the frequency of the detected photons means that the temporal resolution inevitably ceases to be perfect, and antibunching gets lost as a consequence. Emission spectra are typically Lorentzian, i.e., with fat tails and thus regularly emitting arbitrarily far from the central frequency. Since all detectors have a finite bandwidth, such photons are lost. Detection is therefore fundamentally limited in its frequency range or, equivalently, in its temporal resolution. Formally, such an effect is embodied in the expressions for the first- and second-order physical spectra, given in Eqs. (21) and (23), respectively. Thus, the frequency-resolved second-order correlation function is obtained as

$$g^{(2)}_{\Gamma_1\Gamma_2}(\omega_1, T_1; \omega_2, T_2) = \frac{S^{(2)}_{\Gamma_1\Gamma_2}(\omega_1, T_1; \omega_2, T_2)}{S^{(1)}_{\Gamma_1}(\omega_1, T_1) S^{(1)}_{\Gamma_2}(\omega_2, T_2)}, \quad (33)$$

which is the counterpart of Eq. (2) for photons whose frequencies ω_i as well as times T_i of detections are now known within the limits Γ_i of the detectors.

Obtaining the frequency-resolved correlations in Eq. (33) is a complicated task, for which several integrals must be performed, keeping track of the integration regions that stem from the time-ordering requirements. Even for the most fundamental system, the two-level system, and a detection function with an exponential profile [as given in Eq. (29)], this endeavor required some approximations that however allowed one to obtain approximate analytical expressions [45,80–85].

A theory to compute N-photon frequency-resolved photon correlations [56], for which Eq. (33) is a particular case with $N = 2$, was shown to be both exact and simple to implement. It consists in adding detectors to the source of light, whose correlations recover those of the filtered emission of the source. This is exact provided the dynamics of the detectors do not perturb that of the source itself. This can be ensured either by having the source and the detectors coupled with a vanishing strength (this was actually the approach taken in the original paper [56]) or by turning to the cascaded formalism [86,87], by which the coupling is unidirectional and the detectors become the targets of the excitation of the source of light, which remains unaffected by the presence of the detectors. We have shown that, for Glauber correlations, these two approaches are equivalent [88] (to measure, say, the numerators of the Glauber correlators, of which the population is a particular case of interest, the cascading formalism must be used). In practical terms, the description of the system consisting of the source and the detectors of the emission that will implement frequency filtering, as shown in Ref. [56], is done by augmenting the master equation, namely, Eq. (10) for incoherent pumping and Eq. (13) for coherent driving, with a detector described by a bosonic operator ξ. Thus, if the source of light is described by a field with annihilation operator σ (which in our case is the two-level system but
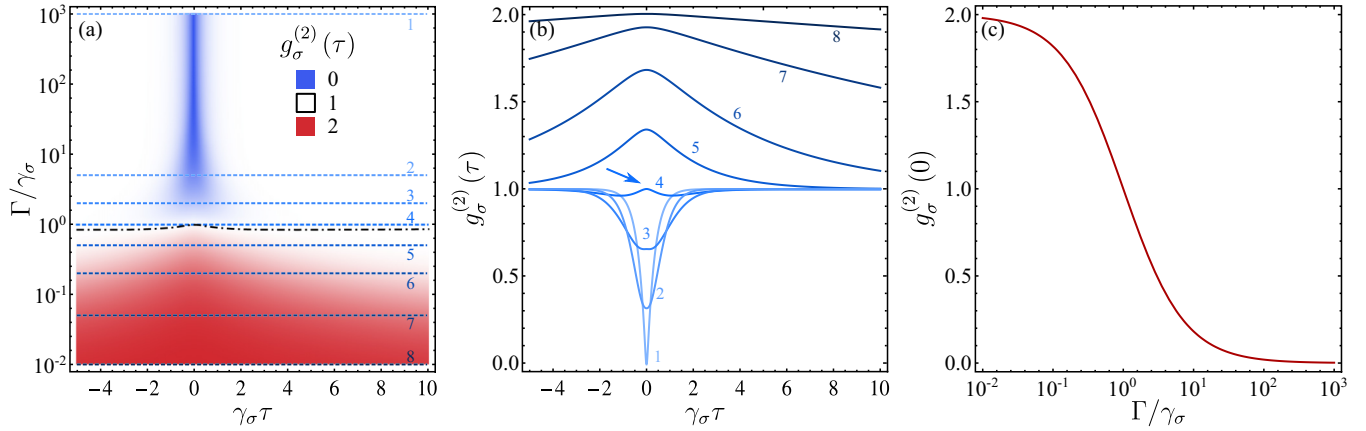
FIG. 4. Loss of antibunching of an incoherently driven 2LS due to frequency filtering. (a) The observed correlations transit from perfect antibunching when not filtering ($\Gamma \to \infty$) to a complete thermalization in the opposite limit ($\Gamma \to 0$), as described by Eq. (35). (b) Cuts of the map in (a) for the Γ/γ_σ ratios highlighted by the blue dashed lines numbered 1–8. Note that while the correlations vary from antibunching to bunching, they do not pass through an exactly uncorrelated emission, as is evidenced by the lump in the correlations marked by the arrow on line 4. (c) Zero-delay correlation as a function of the linewidth of the detector, showing a smooth loss of antibunching with frequency filtering.

could be any other operator with any given quantum algebra), then the Hamiltonian H for the source is supplemented with a Jaynes-Cummings type of coupling with the detector as (still with $\hbar = 1$)

$$H \to H + \omega_\xi \xi^\dagger \xi + \epsilon(\sigma^\dagger \xi + \xi^\dagger \sigma), \qquad (34)$$

where H is, in our case, either H_σ for incoherent pumping [cf. Eq. (9)] or H_{Ω_σ} for coherent driving [cf. Eq. (12)], ω_ξ is the frequency at which the detector is collecting the light, and ϵ is the (vanishing) strength of the coupling between the source and the detector. In addition, the bandwidth Γ of the detector ξ is included thought a Lindblad term $\mathcal{L}_\xi \rho = (\Gamma/2)(2\xi \rho \xi^\dagger - \xi^\dagger \xi \rho - \rho \xi^\dagger \xi)$. Given that the operator ξ describes the detector of light, the parameter Γ can also be interpreted as the *linewidth* of the detector. Note that if the detector were in isolation (without coupling it to the source), its emission spectrum would be given by a Lorentzian of width Γ centered at ω_ξ. Therefore, the frequency filtering done with this detector has a Lorentzian profile and the time resolution is lost following an exponential distribution with mean

$1/\Gamma$. As we will see, that nevertheless leads to a different loss of antibunching than from the corresponding jitter case (cf. Appendix A 2). The method outlined above can also be used to describe detectors with different temporal and spectral resolutions, such as the ones that we have considered in the preceding section: One simply has to couple the source of light to a quantum object whose emission spectrum has the desired shape. However, their implementation is more involved [89] and therefore in this paper we will restrict the discussion to the case of Lorentzian filters.

The rest of the section is devoted to the explicit application of the theory of frequency-resolved correlations to the emission of a two-level system, considering the excitation from both an incoherent and a coherent source of light.

A. Incoherent excitation

The master equation in Eq. (10) with the Hamiltonian in Eq. (9) complemented with a detector ξ of bandwidth Γ gives access to the frequency-resolved correlations of the incoherently driven 2LS. When the detector is in resonance to the 2LS, i.e., $\omega_\xi = \omega_\sigma$, we find

$$g_\sigma^{(2)}(\tau) = 1 - \left(\frac{\Gamma}{\Gamma - \Gamma_\sigma}\right)^2 e^{-\Gamma_\sigma \tau} + \frac{\Gamma_\sigma(\Gamma_\sigma^2 - 3\Gamma\Gamma_\sigma - 2\Gamma^2)}{(\Gamma_\sigma - \Gamma)^2(\Gamma_\sigma + 3\Gamma)} e^{-\Gamma \tau} + \frac{2\Gamma_\sigma \Gamma(5\Gamma - \Gamma_\sigma)}{(\Gamma_\sigma - \Gamma)^2(\Gamma_\sigma + 3\Gamma)} e^{-(\Gamma_\sigma + \Gamma)\tau/2}, \qquad (35)$$

where $\Gamma_\sigma = \gamma_\sigma + P_\sigma$. This result was already obtained through numerical calculations with frequency-resolved Monte Carlo simulations in Ref. [88]. The expressions for higher-order correlations can also be obtained in closed form, but they become bulky and typically not considered for antibunching, so we do not discuss them here. Furthermore, in Ref. [22] we provided a recurrence relation for all correlations at zero delay. The expression in Eq. (35) is written for positive values of τ, but, as before, these correlations are a symmetric function of time, namely, $g_\sigma^{(2)}(\tau) = g_\sigma^{(2)}(-\tau)$, as is shown in Fig. 4. There one can appreciate the transition from perfect antibunching (in the limit in which the linewidth of the detector

is infinite, $\Gamma \to \infty$, and one does not have information about the frequency of the observed photons) to photon bunching (in the opposite regime, where the linewidth of the detector is much smaller than the linewidth of the emission, $\Gamma/\gamma_\sigma \to 0$), where the extreme frequency filtering yields a thermalization of the signal [22,57,90,91]. This is even more clear from the particular case of Eq. (35) at zero delay, which reduces to

$$g_\sigma^{(2)}(0) = \frac{2\Gamma_\sigma}{\Gamma_\sigma + 3\Gamma} \qquad (36)$$

and is shown in Fig. 4(c) [this was also obtained in Ref. [91], Eqs. (6) and (8), and from the cascaded formalism in Ref. [92],

Eq. (14b)]. This displays a smooth transition from antibunching to bunching, in accordance with the universal behavior of thermalization by extreme filtering and of recovering the unfiltered correlations when detecting at all frequencies, namely,

$$\lim_{\Gamma \to 0} g_\sigma^{(2)}(\tau) = 2, \quad \lim_{\Gamma \to \infty} g_\sigma^{(2)}(\tau) = g^{(2)}(\tau) \text{ of Eq. (11).} \quad (37)$$

A series expansion of Γ around zero gives the time dependence for the correlation function for vanishing filters as $g^{(2)}(\tau) \approx 1 + \exp(-\Gamma\tau)$, showing how in this case the dynamics of the emitter itself is completely washed out by the filter, which is solely responsible for the statistics of the surviving photons. The limit of vanishing frequency filtering thus deviates qualitatively from the case considered in the preceding section, where the loss of antibunching was due to temporal uncertainty in the measurement. Here we observe thermalization, with $g_\sigma^{(2)}(0) = 2$, while in the latter case we observed that the signal became uncorrelated, with $\lim_{\Gamma \to 0} g_\Gamma^{(2)}(\tau) = 1$, regardless of the jitter function. This highlights the fundamental difference between the two mechanisms through which the antibunching is lost, with the randomization in the case of temporal uncertainty and the indistinguishability bunching stemming from frequency filtering [91].

Looking more closely, the isoline $g_\sigma^{(2)}(\tau) = 1$ is not straight in Fig. 4(a) (black dash-dotted line). Cuts for some values of the detector linewidth are shown in Fig. 4(b), where the various numbered lines correspond to the horizontal dashed lines in Fig. 4(a). Thus, the transition of the correlations from antibunching to a thermal state with an increase of the coherence time, as filtering tightens, does not transit through exactly uncorrelated (or coherent) light. The shape is similar to that of an antibunched signal contaminated by thermal noise with a smaller coherence time [cf. Eq. (19)] and possibly the effect of the filter could be understood in these terms: converting some photons from the signal into thermal photons. The transition is thus richer than one could have expected. Therefore, Eq. (37) should be more accurately used than the customary single-exponential fit $g^{(2)}(\tau) \approx 1 - g_0^{(2)} \exp(-t/\tau_0)$, where the value

of the parameter g_0 is introduced from a deconvolution of the photon correlations with the temporal profile of the instrument response function [29,59–79]. The observation of this detailed structure of the loss of antibunching seems to be readily observable experimentally and would provide a fundamental test of the theory of frequency-resolved photon correlation from one of the most basic types of quantum emission as well as confirm that the loss of antibunching is more complex and varied than is typically assumed, even for the most simple cases.

B. Coherent excitation

Now turning to the master equation (13) complemented by a detector ξ, we obtain the time-resolved frequency-resolved correlations for the coherently driven 2LS. The general expression can also be obtained analytically, but it becomes quite cumbersome and will require the definition of a few auxiliary notations. It takes the form of a sum of seven exponentials of τ correcting the no-correlation value (unity)

$$g_\sigma^{(2)}(\tau) = 1 + \sum_{i=1}^{7} \mathcal{G}_i^{(2)} \exp(-\gamma_i \tau) \quad (38)$$

with coherence times

$$\gamma_1 \equiv (3\gamma_\sigma + \gamma_M)/4, \quad \gamma_2 \equiv (3\gamma_\sigma - \gamma_M)/4, \quad (39a)$$

$$\gamma_3 \equiv \Gamma/2, \quad (39b)$$

$$\gamma_4 \equiv \gamma_{11}/2, \quad (39c)$$

$$\gamma_5 \equiv (\gamma_{23} + \gamma_M)/4, \quad \gamma_6 \equiv (\gamma_{23} - \gamma_M)/4, \quad (39d)$$

$$\gamma_7 \equiv \Gamma, \quad (39e)$$

where we have introduced the notation

$$\gamma_{ij} \equiv i\Gamma + j\gamma_\sigma, \quad (40)$$

i.e., $\gamma_{11} = \Gamma + \gamma_\sigma$ and $\gamma_{23} = 2\Gamma + 3\gamma_\sigma$. The corresponding coefficients $\mathcal{G}_i$ are bulky and given in Eqs. (B1)–(B7), but various limits of interest can be obtained in closed form of size reasonable enough to be featured as complete expressions, starting with the zero-delay correlation for arbitrary driving intensities:

$$g_\sigma^{(2)}(0) = \frac{\gamma_{11}(\gamma_{01}^2 + 4\Omega_\sigma^2)(\gamma_{11}\gamma_{12} + 8\Omega_\sigma^2)\left[\gamma_{11}\gamma_{21}^2\gamma_{31}^2\gamma_{12}\gamma_{32} + 4\gamma_{10}\gamma_{31}(17\gamma_{10}^3 + 29\gamma_{10}^2\gamma_{01} + 18\gamma_{10}\gamma_{01}^2 + 4\gamma_{01}^3)\Omega_\sigma^2 + 48\gamma_{10}^2\gamma_{21}\Omega_\sigma^4\right]}{\gamma_{21}\gamma_{31}(\gamma_{11}\gamma_{21} + 4\Omega_\sigma^2)(\gamma_{31}\gamma_{32} + 8\Omega_\sigma^2)(\gamma_{11}^2\gamma_{12} + 4\gamma_{10}\Omega_\sigma^2)^2}. \quad (41)$$

This was also obtained from the cascaded formalism in Ref. [92], Eq. (19b), and used to account for finite-driving departures in Ref. [46], where this expressions provided an essentially exact fit to the raw data.

The time correlations in the low-driving Heitler limit can be considerably simplified,

$$g_{\sigma,\text{Heitler}}^{(2)}(\tau) = \frac{e^{-(\Gamma + \gamma_\sigma)\tau}\left[\Gamma^2 e^{\Gamma\tau/2} - \Gamma\gamma_\sigma e^{\gamma_\sigma\tau/2} - (\Gamma^2 - \gamma_\sigma^2)e^{(\Gamma+\gamma_\sigma)\tau/2}\right]^2}{(\Gamma^2 - \gamma_\sigma^2)^2}, \quad (42)$$

with a simple overall behavior of a monotonic loss of antibunching, due to frequency filtering, given by

$$g_{\sigma,\text{Heitler}}^{(2)}(0) = \left(\frac{\gamma_\sigma}{\gamma_\sigma + \Gamma}\right)^2. \quad (43)$$

This is shown on Fig. 5(a). The zero-delay correlation function was obtained in Ref. [91], Eq. (21). The high-driving Mollow regime, on the other hand, is more complex. In particular, taking the limit $\Omega_\sigma \to \infty$ sends the satellite peaks away and, if
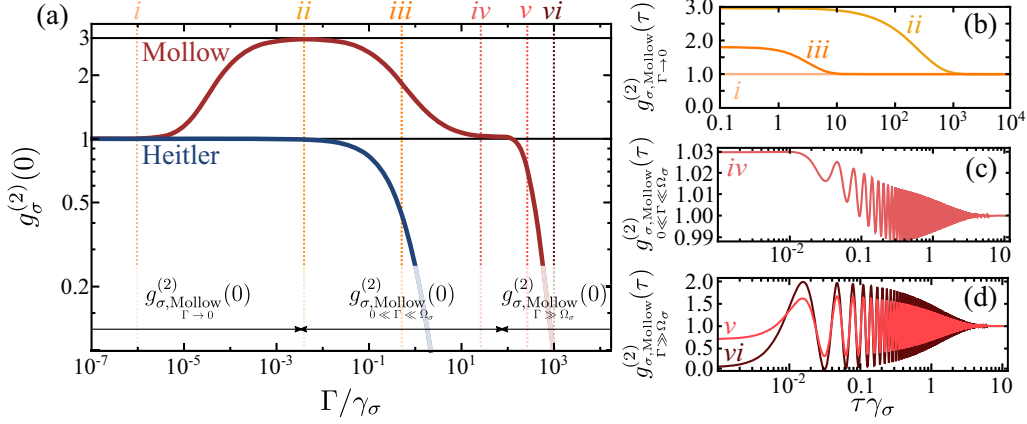
FIG. 5. Loss of antibunching for the coherently driven 2LS in the Heitler ($\Omega_\sigma/\gamma_\sigma \to 0$) and deep Mollow ($\Omega_\sigma/\gamma_\sigma = 100$) regimes, both at (a) zero delay and (b)–(d) as a function of time τ in the various limits of the Mollow triplet ($\Omega_\sigma \gg \gamma_\sigma$) depending on the filter widths: (b) when Γ is small, exhibiting bunching; (c) at intermediate Γ, with onset of correlations; and (d) when Γ is large and beyond the triplet splitting, exhibiting antibunching. Note the very different scales on both axes of (b)–(d). Case iii, which belongs to the intermediate regime, displays a correlation function akin to those of the low-Γ case and is best plotted with them. These results can be obtained either from Eqs. (41)–(48) in the corresponding limits or from Eq. (38), which covers all the cases simultaneously (but through a very bulky expression).

$\Gamma \to \infty$ slower than Ω_σ, filtering will be limited to the central peak in this case, which cannot produce values below 1, namely,

$$g^{(2)}_{\substack{\sigma,\text{Mollow}\\0\ll\Gamma\ll\Omega_\sigma}}(\tau) = 1 + 2\gamma_\sigma \frac{2\Gamma e^{-(\Gamma+\gamma_\sigma)\tau/2} - (\Gamma + \gamma_\sigma)e^{-\Gamma\tau}}{(\Gamma - \gamma_\sigma)(3\Gamma + \gamma_\sigma)}, \tag{44}$$

with zero-delay coincidences

$$g^{(2)}_{\substack{\sigma,\text{Mollow}\\0\ll\Gamma\ll\Omega_\sigma}}(0) = \frac{3(\Gamma + \gamma_\sigma)}{3\Gamma + \gamma_\sigma}. \tag{45}$$

This corresponds to Fig. 5(c). The other cases, namely $\Gamma \to 0$ [Fig. 5(b)] and $\Gamma \to \infty$ faster than Ω_σ [Fig. 5(d)], have to be treated independently and retain the Ω_σ dependence, to yield [here we upgrade the notation (40) with a bar to refer to a negative number, e.g., $\gamma_{2\bar{1}} = 2\Gamma - \gamma_\sigma$, and with a comma if involving two-digit integers, e.g., $\gamma_{14,\bar{5}} = 14\Gamma - 5\gamma_\sigma$]

$$g^{(2)}_{\substack{\sigma,\text{Mollow}\\\Gamma\to 0}}(\tau) = 1 + \left(\frac{2\gamma_\sigma^2}{\Omega_\sigma^2} + \frac{4\Gamma\gamma_{2\bar{1}}}{\gamma_\sigma^2}\right)e^{-(\Gamma+\gamma_\sigma)\tau/2} + \frac{3\gamma_\sigma^8 - 8\Gamma\gamma_\sigma^4\gamma_{11}\Omega_\sigma^2 + 16\Gamma^2(\Gamma\gamma_{5\bar{1}} + \gamma_\sigma^2)\Omega_\sigma^4}{8\Gamma^2\gamma_\sigma^2\Omega_\sigma^4}e^{-\Gamma\tau}, \tag{46a}$$

$$\begin{aligned}g^{(2)}_{\substack{\sigma,\text{Mollow}\\\Gamma\gg\Omega_\sigma}}(\tau) &= 1 + \frac{8(\Gamma/\Omega_\sigma)^2[10 + (\Gamma/\Omega_\sigma)^2]}{[4 + (\Gamma/\Omega_\sigma)^2][8 + (\Gamma/\Omega_\sigma)^2]^2}e^{-\Gamma\tau} - \frac{4(\Gamma/\Omega_\sigma)^2[16 + (\Gamma/\Omega_\sigma)^2]}{[4 + (\Gamma/\Omega_\sigma)^2][8 + (\Gamma/\Omega_\sigma)^2]^2}e^{-(\gamma_\sigma+\Gamma)\tau/2}\\[4pt] &\quad + \frac{4(\Gamma/\Omega_\sigma)^2\{[16 + (\Gamma/\Omega_\sigma)^2]\cos(2\Omega_\sigma\tau) + (\Gamma/\Omega_\sigma)[10 + (\Gamma/\Omega_\sigma)^2]\sin(2\Omega_\sigma\tau)\}}{[4 + (\Gamma/\Omega_\sigma)^2][8 + (\Gamma/\Omega_\sigma)^2]^2}e^{-(3\gamma_\sigma+2\Gamma)\tau/4}\\[4pt] &\quad - \frac{(\Gamma/\Omega_\sigma)^2[16 + (\Gamma/\Omega_\sigma)^2]\cos(2\Omega_\sigma\tau)}{[8 + (\Gamma/\Omega_\sigma)^2]^2}e^{-3\gamma_\sigma\tau/4},\end{aligned} \tag{46b}$$

with the latter highly oscillating function being enclosed by the envelopes

$$g^{(2)}_{\substack{\sigma,\text{Mollow}\\\Gamma\gg\Omega_\sigma}}(\tau) = 1 \pm \frac{(\Gamma/\Omega_\sigma)^2[16 + (\Gamma/\Omega_\sigma)^2]}{[8 + (\Gamma/\Omega_\sigma)^2]^2}e^{-3\gamma_\sigma\tau/4} \tag{47}$$

and with zero-delay correlations

$$g^{(2)}_{\substack{\sigma,\text{Mollow}\\\Gamma\to 0}}(0) = \frac{\gamma_{41}\gamma_\sigma^9 + 12\Gamma\gamma_{21}\gamma_\sigma^6\Omega_\sigma^2 - 16\Gamma^2\gamma_\sigma^3\gamma_{14,\bar{5}}\Omega_\sigma^4 - 192\Gamma^3\gamma_{2\bar{1}}\Omega_\sigma^6}{\gamma_\sigma(\gamma_\sigma^3 + 4\Gamma\Omega_\sigma^2)^3} \to 1 + \frac{4\gamma_\sigma}{\Gamma}, \tag{48a}$$

$$g^{(2)}_{\substack{\sigma,\text{Mollow}\\\Gamma\gg\Omega_\sigma}}(0) = \frac{8[2 + (\Gamma/\Omega_\sigma)^2][16 + (\Gamma/\Omega_\sigma)^2]}{[4 + (\Gamma/\Omega_\sigma)^2][8 + (\Gamma/\Omega_\sigma)^2]^2} \to \frac{8\Omega_\sigma^2}{\Gamma^2} \tag{48b}$$

that correspond to the left and right parts of Fig. 5(a), respectively. The simplest formula we can find that unites all these behaviors is the one that is valid for all Ω_σ anyway, namely, Eq. (41) to describe the three limits of Eqs. (48a), (45), and (48b) that together reconstruct completely the curve in Fig. 5(a), and, for the τ dependence, Eq. (38) along with (39) and (B1)–(B7) for the corresponding limits of Eqs. (46a), (44), and (46b).
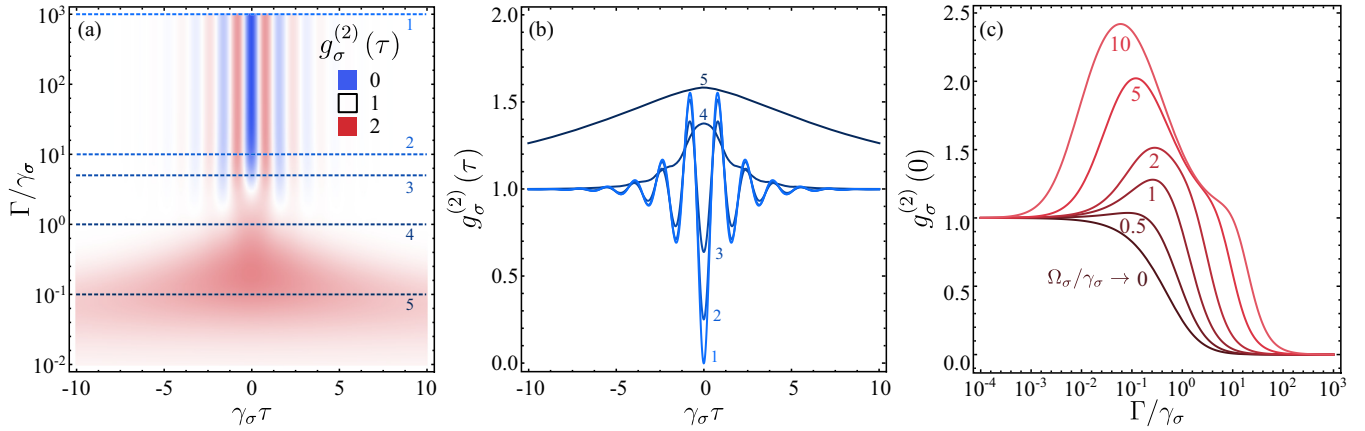
FIG. 6. Loss of antibunching of a coherently driven 2LS due to frequency filtering. (a) The Rabi oscillations induced by the laser are dampened by the frequency filtering, and the perfect antibunching obtained in the limit $\Gamma \to \infty$ thermalizes when $\Gamma = \gamma_\sigma$. However, further reducing the linewidth of the detector reveals the uncorrelated nature of the light emitted by the driving laser. (b) Cuts of the density plot in (a) illustrating the transition between these regimes. (a) and (b) correspond to $\Omega_\sigma = 2\gamma_\sigma$. (c) Zero-delay correlations on the low side $\Omega_\sigma/\gamma_\sigma$ of the Mollow triplet, down to its disappearance at $\Omega_\sigma/\gamma_\sigma = 1/\sqrt{8}$, at which point bunching disappears.

Some of the above results are still quite heavy, but that only illustrates how rich and complex the seemingly simple and basic problem of filtering a two-level system is and the sort of complexity needed to embody all these various regimes and behaviors in a single analytical expression. One can check indeed that these results recover those of the unfiltered case in the limit $\Gamma \to \infty$, namely, Eq. (46b) recovers Eq. (14), Eq. (47) recovers Eq. (16), and Eq. (42) recovers Eq. (15), while their respective $\tau = 0$ cases, Eqs. (48b) and (43), both recover the perfect antibunching $g_\sigma^{(2)}(0) = 0$. Frequency filtering allows us to see how both the Heitler and Mollow antibunching go to zero with the same speed with filtering, namely, as its inverse square, but that the necessity to first go over the bunching of the central peak of the Mollow triplet delays the antibunching phase so that the Heitler regime always keeps the upper hand, as seen in Fig. 5. It is also instructive to observe that the bulk of the complexity lies with the antibunching of the Mollow regime (46b), which overall seems more predisposed to emit bunched light, confirming its key role in multiphoton physics [93]. In all instances, the results are particular cases of Eq. (38) [with its coefficients (B1)–(B7) and decay rates (39)].

The characteristic shapes of $g_\sigma^{(2)}(0)$ shown in Fig. 5(a) were also discussed in Ref. [91]. The two plateaus $g_\sigma^{(2)}(0) = 1$ in the Mollow case, which sandwich the plateau $g_\sigma^{(2)}(0) = 3$, are of a different nature. At vanishing Γ, one is filtering the coherently scattered light from the laser alone (the so-called Rayleigh peak), which reproduces the laser uncorrelation. However, at larger Γ (though still below Ω_σ), one is fully filtering the central peak of the Mollow triplet. This peak dominates the correlations because the coherent fraction is much smaller in the Mollow regime. Considering the transitions between dressed states that produce the central peak, one would expect bunching in this regime, but due to an interference between the two possible deexcitation paths, correlations go down to $g_\sigma^{(2)}(0) = 1$ again, as explained in Ref. [91] and references therein. The intermediate plateau at $g_\sigma^{(2)}(0) = 3$ is obtained for filtering widths smaller than γ_σ but larger than $\Gamma_\sigma^3/(4\Omega_\sigma^2)$ [91], a point at which the coherent part (Rayleigh peak) equals

the incoherent part (central peak of the Mollow triplet). In this regime, the interference no longer holds and the expected bunching manifests. More specifically, the value of 3 suggests that the central peak of the Mollow triplet corresponds to squeezed light [54]. Such a particular value is not yet, but could become, a typical value of Glauber correlations along with 0 (antibunching), 1 (uncorrelated or laser), and 2 (thermal), as the value realized under extreme squeezing. Such a rich span of a wide range of photon correlations in the deep Mollow regime remains to be observed experimentally.

We also show temporal correlations for the coherently driven single-photon source in the lower Ω_σ/Γ side of the Mollow regime ($\Omega_\sigma = 2\gamma_\sigma$) in Fig. 6(a), which is more relevant for experiments, as a function of time and of the linewidth of the detector, i.e., as a counterpart of Fig. 4. This puts in better perspective the several and striking differences with respect to the case of incoherent driving. First is the presence of Rabi oscillations induced by the laser, which are maintained, including their frequency, as long as antibunching is observed. They have a maximum visibility when the detector is colorblind [94], in which case they recover Eq. (14). Figure 6(b) shows a series of cuts for several values of Γ/γ_σ, marked in Fig. 6(a) by dashed lines, showing how the Rabi oscillations amplitudes are softened and remain reminiscent in the bunching phase, vanishing completely when the detector filters within a region narrower than the linewidth of the 2LS. Second, the limit of vanishing filtering width leads to randomization rather than to thermalization, thereby behaving like a time jitter rather than thermal filtering. This is the same manifestation as for the deep Mollow regime, namely, due to the approximation of the laser as a δ function, which has exactly zero linewidth. One can therefore never filter the photons from within the emission line of the laser, and the thermalization does not appear [91]. However, turning to more sophisticated models of the laser, e.g., the one-atom laser [48], one then reaches a thermalization in the limit $\Gamma \to 0$. The widely used approximation of the laser as a δ function has nevertheless been shown to be good to account for experimental observations several times and under different conditions:

mapping the two- and three-photon correlation landscape of the 2LS [95,96] (in agreement with the theoretical predictions [91,97]) and recently by measuring the effect of the filter [46] in perturbing the balance between the quantum emission and the laser itself in a self-homodyning picture [98]. In this case, when the linewidth of the filtering is not vanishing but still remains below the natural linewidth of the 2LS, the correlations become bunched as the intensity of the driving increases. This brings us to the third main departure from the incoherent case, which was also featured in the deep Mollow regime but that persists as long as the triplet is resolved, namely, the nonmonotonic evolution of $g_\sigma^{(2)}(0)$, even if it would thermalize at vanishing Γ. This is clear when focusing on the zero-delay correlations (41), as shown in Fig. 6(c) as a function of the linewidth of the detector for several intensities of the driving. One can find a region of superbunching with more bunched photons emitted by the 2LS than thermal light itself. Bunching is realized when entering the Mollow triplet regime, i.e., when the intensity of the driving becomes such that the emission spectrum of the 2LS is given by the sum of three Lorentzians [92], when $\Omega_\sigma/\gamma_\sigma \geqslant 1/\sqrt{8}$. This does mean that the triplet itself is spectrally resolved, which happens at about $\Omega_\sigma/\gamma_\sigma \sim 2$. The low-driving case observed experimentally by two independent groups [46,79] featured departures from the Heitler limit $\Omega_\sigma/\gamma_\sigma \to 0$ but still without evidencing bunching. Filtering below the natural linewidth of the 2LS in the Mollow regime means that one is filtering the photons coming from the central peak, which has long been predicted to display bunching [84,91,99] and has since been observed experimentally [95]. While bunching values in excess of 2 appear to be already within experimental reach, the maximum possible bunching $g_\sigma^{(2)}(0) = 3$ is obtained in the strongly filtered, deep Mollow regime, as seen in Fig. 5 and highlighted in Fig. 7. This should make this limit much more difficult to approach.

We do not discuss further the underlying physics of the filtered Mollow triplet [97] as this relates to bunching rather than antibunching, which comes with specificities of its own, but this serves to illustrate how the regime of driving results in very different dynamics for the antibunching of the emitter. In particular, the loss of antibunching is so serious for the coherently driven 2LS that it is complete at all driving intensities, if the filtering is too stringent.

VIII. CONCLUSION AND OUTLOOK

We have described a variety of mechanisms—in our understanding, the most common and important ones—that lead to a reduction of antibunching, namely, contamination by noise (Sec. V), by a time jitter in the photon detection (Sec. VI), and by frequency filtering (Sec. VII). In all cases, we have applied the results to a two-level system under various types and regimes of excitation. The first two mechanisms (noise and jitter) act directly on $g^{(2)}(\tau)$ of the source [through Eq. (19) and the noise-to-signal ratio ξ on the one hand and through Eq. (27) and the jitter function D_Γ on the other hand], while the third one (frequency filtering) depends, at a more fundamental level, on the dynamics of the emitter. As a result, although the theoretical derivations are tightly linked [namely, Eqs. (21) and (23) are the starting point for Eq. (33)], the
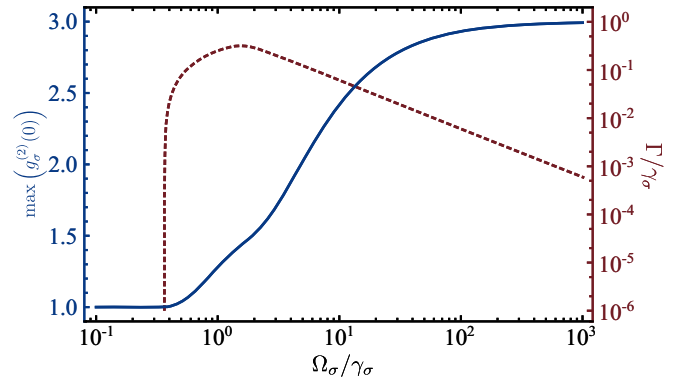
FIG. 7. The blue solid line shows the maximum value that the zero-delay correlation $g_\sigma^{(2)}(0)$ of the coherently driven 2LS can take for a given driving intensity Ω_σ. At every intensity of the driving, the filter's linewidth Γ has been taken to maximize $g_\sigma^{(2)}(0)$ and is shown by the red dashed line with values on the right axis. This shows that a coherently driven 2LS can always fail to display antibunching depending on the filtering. At $\Omega_\sigma/\gamma_\sigma \lesssim 0.4$, the filter's width gets too small to still be featured on the plot but theoretically exists and still remains larger than the δ function (which has no width) as to produce uncorrelated photons. The qualitative change at about $\Omega_\sigma/\gamma_\sigma \sim 2$ occurs when the three peaks of the Mollow triplet start to be spectrally distinguished.

end results differ substantially. For instance, a time jitter can only drive correlations towards uncorrelation, while frequency filtering can alter their type, e.g., turning antibunching into bunching. While the textbook results of the antibunching of a 2LS [Eqs. (11) and (14)] provide a convenient and relevant illustration for the general theory, they become problems of great intrinsic and fundamental interest when turning to their frequency filtering. For the time jitter, we find that while its actual type has only a small quantitative effect, the dynamics of $g^{(2)}(\tau)$ itself is important to characterize the robustness of the correlations to time fluctuations. The low-driving coherent case is overall less affected than its high-driving or incoherent counterparts.

While the formalism for frequency filtering has been considerably studied, including for the 2LS, its link and application to time fluctuations of the jitter type have not been previously considered, and we have introduced the formalism for the loss of antibunching in this case. Regarding frequency filtering, while many numerical simulations and several limiting analytical cases have indeed been provided throughout the years, our present results offer a complete description of the antibunching from a 2LS that unifies all the previous knowledge with closed-form and general analytical expressions which cover all types [incoherent, Eq. (35), and coherent, Eq. (38)] as well as all regimes (low, intermediate, and high) of driving, also being valid for arbitrary time delays as opposed to only coincidences. The incoherent case has very recently benefited from such a generalization by another group [100], relying on a different approach (out of time ordering) and going beyond Lorentzian filtering. The coherent case is very bulky with its full form to be found in Appendix B, but simplifications can be obtained in the low- (Heitler) driving limit (42) and in the high- (Mollow)

driving limit. In the latter case, one should further consider various cases depending on whether Γ is commensurable with [Eq. (44)], much smaller than [Eq. (46a)], or much greater than [Eq. (46b)] the Mollow splitting. Since the 2LS is a textbook system, such a comprehensive description of its antibunching is naturally desirable in addition to its importance for a detailed characterization at both a fundamental and applied level. Many of our results apply directly to other cases, including both other systems and other types of photon statistics. For instance, it would be instructive to adapt this analysis to the current record holders of antibunched emission [6,7] and track whether the origin of the remaining imperfection lies in the factors analyzed here or in the source itself (i.e., residual reexcitation). Ultimately, failures attributed to the source really belong to the detection scheme as a better detector with a higher time resolution would be able to discriminate photon pairs in time and their antibunching, although these could be attributed to a mechanism inherent to the source, such as its reexcitation. In this regard, we have already speculated that a perfect antibunched source should not have a Lorentzian profile [92] but feature a standard deviation so as to avoid spurious coincidences from the finite bandwidth of the detector, which is unavoidable. The design of such a perfect source in itself, however, constitutes a different problem.

Even the 2LS system that we have studied in this text could be analyzed further, e.g., to higher photon orders, out of resonance with the filter (in particular for the Mollow triplet), including other processes such as pure dephasing or phonon-induced dephasing, etc. One could also extend the discussion to other mechanisms that spoil antibunching (some, such as the gravity peak of a streak camera whereby one photon spreads over several pixels of the detectors, are covered in Ref. [42]) or combine those that we have discussed, from loss by external noise, time uncertainty, and/or frequency filtering. There are indeed more mechanisms leading to a loss of antibunching than one would actually want to account for, and none of them consists in a simple exponential damping of the perfect antibunching of the source. While one particular mechanism (frequency filtering) has been recently investigated in depth for one of the regimes considered above (close to the Heitler regime) [46,79], there remains much to investigate experimentally. In particular, the Mollow triplet, although rooted in a 2LS, proves to be particularly apt at emitting a variety of bunched light and even its coherent emission can arise from different mechanisms. The observation of the zero-delay photon correlations shown in Fig. 5 along with time correlations would span a large range of basic regimes of quantum optical emission. This would provide an instant classic illustration of the versatility and complexity of an otherwise extremely basic and simple system. Also, the transition from antibunching to bunching for the incoherently driven two-level system, tending to thermalization ruled by the filter alone and passing by an imperfectly uncorrelated state exhibiting a small suppression of photon pairs within the emitter's coherence time when $g^{(2)}(0) = 1$, still remains a considerable omission from experimental characterizations of what is arguably the most widely and commonly studied quantum optical emitter. The level of agreement with the theory would allow one to assess how valid the two-level picture is for the emitter in question, how well understood the mechanism leading to its loss of antibunching is, and, at a more fundamental level, how accurate the theory of frequency-resolved photon correlations is, which constitutes in itself a basic aspect of the theory of photodetection.

APPENDIX A: TIME JITTER

1. Heaviside function

The case of the Heaviside function (28) yields, for Eq. (27),

$$g_\Gamma^{(2)}(\tau) = \Gamma \int_\tau^{\tau+1/\Gamma} dx\, g^{(2)}(x)[1 - \Gamma(x-\tau)] + \theta\left(\tau - \frac{1}{\Gamma}\right)\Gamma \int_{\tau-1/\Gamma}^{\tau} dx\, g^{(2)}(x)[1 + \Gamma(x-\tau)]$$

$$+ \theta\left(\frac{1}{\Gamma} - \tau\right)\Gamma\left\{\int_0^{1/\Gamma-\tau} dx\, g^{(2)}(x)[1 - \Gamma(x+\tau)] + \int_0^\tau dx\, g^{(2)}(x)[1 + \Gamma(x-\tau)]\right\}, \tag{A1}$$

providing the photon correlations from an incoherently driven 2LS with time jitter,

$$g_{\Gamma,P_\sigma}^{(2)}(\tau) = 1 - \frac{\Gamma^2}{\Gamma_\sigma^2} e^{-\Gamma_\sigma(\tau+1/\Gamma)}(1 - e^{\Gamma_\sigma/\Gamma})^2 \theta\left(\tau - \frac{1}{\Gamma}\right)$$

$$- \frac{2\Gamma^2}{\Gamma_\sigma^2}\left\{e^{-\Gamma_\sigma/\Gamma}\cosh(\Gamma_\sigma\tau) - e^{-\Gamma_\sigma\tau} + \Gamma_\sigma\left(\frac{1}{\Gamma} - \tau\right)\right\}\theta\left(\frac{1}{\Gamma} - \tau\right), \tag{A2}$$

with the $\tau \geqslant 1/\Gamma$ behavior on the first line and $\tau \leqslant 1/\Gamma$ on the second line, while the corresponding expression for the coherently driven 2LS is

$$
\begin{aligned}
g^{(2)}_{\Gamma,\Omega_\sigma}(\tau) = {} & 1 - \frac{32\Gamma^2 e^{-3\gamma_\sigma\tau/4}}{R_\sigma(R_\sigma^2 + 9\gamma_\sigma^2)^2}\left[9\gamma_\sigma(R_\sigma^2 - 3\gamma_\sigma^2)\sin\left(\frac{R_\sigma\tau}{4}\right) + R_\sigma(R_\sigma^2 - 27\gamma_\sigma^2)\cos\left(\frac{R_\sigma\tau}{4}\right)\right] \\
& + \frac{16\Gamma e^{-3\gamma_\sigma\tau/4}e^{-3\gamma_\sigma/4\Gamma}}{R_\sigma(R_\sigma^2 + 9\gamma_\sigma^2)^2}\left[9\gamma_\sigma(R_\sigma^2 - 3\gamma_\sigma^2)\sin\left(\frac{R_\sigma(1 + \Gamma\tau)}{4\Gamma}\right) + R_\sigma(R_\sigma^2 - 27\gamma_\sigma^2)\cos\left(\frac{R_\sigma(1 + \Gamma\tau)}{4\Gamma}\right)\right] \\
& + \frac{16\Gamma^2(R_\sigma^2 - 27\gamma_\sigma^2)}{(R_\sigma^2 + 9\gamma_\sigma^2)^2}\cos\left(\frac{R_\sigma(1 - \Gamma\tau)}{4\Gamma}\right)e^{-3\gamma_\sigma|1-\Gamma\tau|/4\Gamma} - \frac{48\Gamma\gamma_\sigma(1 - \Gamma\tau)}{R_\sigma^2 + 9\gamma_\sigma^2}\theta\left(\frac{1}{\Gamma} - \tau\right) \\
& + \frac{144\Gamma^2\gamma_\sigma(R_\sigma^2 - 3\gamma_\sigma^2)}{R_\sigma(R_\sigma^2 + 9\gamma_\sigma^2)^2}\sin\left(\frac{R_\sigma(1 - \Gamma\tau)}{4\Gamma}\right)\left[e^{-3\gamma_\sigma(1-\Gamma\tau)/4\Gamma}\theta\left(\frac{1}{\Gamma} - \tau\right) - e^{3\gamma_\sigma(1-\Gamma\tau)/4\Gamma}\theta\left(\tau - \frac{1}{\Gamma}\right)\right].
\end{aligned} \tag{A3}
$$

where we have used the notation $R_\sigma \equiv \sqrt{(8\Omega_\sigma)^2 - \gamma_\sigma^2}$.

2. Exponential function

In this case, the correlations with time jitter are given by

$$
g^{(2)}_\Gamma(\tau) = \Gamma\cosh(\Gamma\tau)\int_0^\infty g^{(2)}(x)e^{-\Gamma x}dx - \Gamma\int_0^\tau g^{(2)}(x)\sinh[\Gamma(\tau - x)]dx. \tag{A4}
$$

In the case of the incoherently driven 2LS, the correlations with time jitter become

$$
g^{(2)}_{\Gamma,P_\sigma}(\tau) = 1 - \frac{1}{1 - (\Gamma_\sigma/\Gamma)^2}[e^{-\Gamma_\sigma\tau} - (\Gamma_\sigma/\Gamma)e^{-\Gamma\tau}], \tag{A5}
$$

with the limit $g^{(2)}_{\Gamma,P_\sigma}(\tau) = 1 - e^{-\Gamma_\sigma\tau}(1 + \Gamma_\sigma\tau)/2$ when $\Gamma = \Gamma_\sigma$, whereas the correlations of the coherently driven 2LS become

$$
g^{(2)}_{\Gamma,\Omega_\sigma}(\tau) = 1 - \frac{j_{1,\Omega_\sigma}}{N_+ N_-}e^{-\Gamma\tau} - \frac{j_{2,\Omega_\sigma}}{R_\sigma N_+ N_-}e^{-3\gamma_\sigma\tau/2}, \tag{A6}
$$

where $N_\pm = R_\sigma^2 + (4\Gamma \pm 3\gamma_\sigma)^2$ and we have defined the functions

$$
j_{1,\Omega_\sigma} = 24\Gamma\gamma_\sigma(R_\sigma^2 + 9\gamma_\sigma^2), \tag{A7a}
$$

$$
j_{2,\Omega_\sigma} = 16R_\sigma\Gamma^2(R_\sigma^2 + 16\Gamma^2 - 27\gamma_\sigma^2)\cos\left(\frac{R_\sigma\tau}{4}\right) + 48\Gamma^2\gamma_\sigma(3R_\sigma^2 + 16\Gamma^2 - 9\gamma_\sigma^2)\sin\left(\frac{R_\sigma\tau}{4}\right). \tag{A7b}
$$

3. Double exponential

With this function, the expression for the time jitter correlations is given by

$$
\begin{aligned}
g^{(2)}_\Gamma(\tau) = {} & \Gamma\int_0^\infty dx\, g^{(2)}(x)e^{-2\Gamma x}[(1 + 2x\Gamma)\cosh(2\Gamma\tau) \\
& - 2\Gamma\tau\sinh(2\Gamma\tau)] - \Gamma\int_0^\tau dx\, g^{(2)}(x)\{\sinh[2\Gamma(\tau - x)] \\
& - 2\Gamma(\tau - x)\cosh[2\Gamma(\tau - x)]\}.
\end{aligned} \tag{A8}
$$

In this case, the correlations of the incoherently driven 2LS, with bare correlations given in Eq. (11), become

$$
g^{(2)}_{\Gamma,P_\sigma}(\tau) = 1 - \frac{16}{\Delta^2}e^{-\Gamma_\sigma\tau} + \frac{(\Gamma_\sigma/\Gamma)[8 + \Delta(1 + 2\Gamma\tau)]}{\Delta^2}e^{-2\Gamma\tau}, \tag{A9}
$$

where we have used the notation $\Delta \equiv 4 - (\Gamma_\sigma/\Gamma)^2$. The counterpart for the coherent excitation is given by

$$
g^{(2)}_{\Gamma,\Omega_\sigma}(\tau) = 1 - \frac{g_{1,\Omega_\sigma}}{\mathcal{N}_{\Omega_\sigma}}e^{-3\gamma_\sigma\tau/4} - \frac{g_{2,\Omega_\sigma}}{\mathcal{N}_{\Omega_\sigma}}e^{-2\Gamma\tau}, \tag{A10}
$$

where we have introduced the functions g_{1,Ω_σ}, g_{2,Ω_σ}, and $\mathcal{N}_{\Omega_\sigma}$ as

$$
g_{1,\Omega_\sigma} = 4096\Gamma^4\left[R_\sigma\left[(R_\sigma^2 + 64\Gamma^2)^2 - 18(5R_\sigma^2 + 192\Gamma^2)\gamma_\sigma^2 + 405\gamma_\sigma^4\right]\cos\left(\frac{R_\sigma\tau}{4}\right)\right.
$$

$$+ 3\gamma_\sigma \left[5R_\sigma^4 + 6R_\sigma^2\left(64\Gamma^2 - 15\gamma_\sigma^2\right) + \left(64\Gamma^2 - 9\gamma_\sigma^2\right)^2\right]\sin\left(\frac{R_\sigma \tau}{4}\right)\right], \tag{A11a}$$

$$g_{2,\Omega_\sigma} = 24R_\sigma\Gamma\gamma_\sigma\left(R_\sigma^2 + 9\gamma_\sigma^2\right) + \left\{R_\sigma^4 + 384R_\sigma^2\Gamma^2 + 20\,480\Gamma^4 - 3456\Gamma^2\gamma_\sigma^2 + 81\gamma_\sigma^4\right.$$
$$\left. + 2\Gamma\left[R_\sigma^2 + (8\Gamma - 3\gamma_\sigma)^2\right]\left[R_\sigma^2 + (8\Gamma + 3\gamma_\sigma)^2\right]\tau\right\}, \tag{A11b}$$

$$\mathcal{N}_{\Omega_\sigma} = R_\sigma\left[R_\sigma^4 + 2R_\sigma^2\left(64\Gamma^2 + 9\gamma_\sigma^2\right) + \left(64\Gamma^2 - 9\gamma_\sigma^2\right)^2\right]. \tag{A11c}$$

4. Gaussian

With this function, the correlations with time jitter are given by

$$g_\Gamma^{(2)}(\tau) = \frac{\Gamma}{2\sqrt{\pi}}\int_0^\infty g^{(2)}(x)\left\{e^{-[(\tau+x)\Gamma/2]^2} + e^{-[(\tau-x)\Gamma/2]^2}\right\}dx. \tag{A12}$$

The correlation with time uncertainty for the incoherently driven 2LS becomes

$$g_{\Gamma,P_\sigma}^{(2)}(\tau) = 1 - \frac{e^{(\Gamma_\sigma/\Gamma)^2}}{2}\left\{e^{-\Gamma_\sigma\tau}\mathrm{erfc}(\tau_-) + e^{\Gamma_\sigma\tau}\mathrm{erfc}(\tau_+)\right\}, \tag{A13}$$

where $\mathrm{erfc}(\tau)$ is the complementary error function and we have defined

$$\tau_\pm = \frac{\Gamma_\sigma}{\Gamma} \pm \frac{\Gamma\tau}{2}.$$

The counterpart for coherent excitation has a more complicated structure

$$g_{\Gamma,\Omega_\sigma}^{(2)}(\tau) = 1 - \frac{\Delta_-}{iR_\sigma}e^{(\Delta_+/\Gamma)^2}h_{1,\Omega_\sigma} - \frac{\Delta_+}{iR_\sigma}e^{(\Delta_-/\Gamma)^2}h_{2,\Omega_\sigma}, \tag{A14}$$

where we have introduced the functions $h_{1,\Omega}$ and $h_{2,\Omega}$ and the parameters $\Delta_\pm$, defined as

$$h_{1,\Omega_\sigma} = 2\cosh(\Delta_+\tau) + \mathrm{erf}(\lambda_{1,+})e^{\Delta_+\tau} + \mathrm{erf}(\lambda_{1,-})e^{-\Delta_+\tau}, \tag{A15a}$$

$$h_{2,\Omega_\sigma} = 2\cosh(\Delta_-\tau) - \mathrm{erf}(\lambda_{2,+})e^{\Delta_-\tau} - \mathrm{erf}(\lambda_{2,-})e^{-\Delta_-\tau}, \tag{A15b}$$

where we have used $\Delta_\pm = (iR_\sigma \pm 3\gamma_\sigma)/4$, $\lambda_{1,\pm} = \Delta_+/\Gamma \pm \Gamma\tau/2$, and $\lambda_{2,\pm} = \Delta_-/\Gamma \pm \Gamma\tau/2$ and R_σ is as defined in Eq. (14).

APPENDIX B: FREQUENCY FILTERING

The seven coefficients $\mathcal{G}_i$ which, together with the coherence times (39), yield the general two-photon autocorrelation function $g_\sigma^{(2)}(\tau)$ for the coherently driven 2LS according to Eq. (38) are given below. They also consist of intricate combinations of the various rates involved, this time also involving subtractions, so that we upgrade Eq. (40) as explained in the text with a bar over the number meaning that it is negative:

$$\mathcal{G}_1 \equiv 512\Gamma^2\gamma_{11}\Omega_\sigma^2\left(\gamma_{11}\gamma_{12} + 16\Omega_\sigma^2\right)\left\{\Gamma\gamma_{1\bar{2}}\gamma_{1\bar{1}}(\gamma_M + \gamma_\sigma) + 8[14\Gamma^2 + 2\gamma_\sigma(\gamma_M + \gamma_\sigma) - \Gamma(7\gamma_M + 17\gamma_\sigma)]\Omega_\sigma^2 - 512\Omega_\sigma^4\right\}$$
$$\times \left\{\gamma_{11}\gamma_{12}\gamma_{21}[\Gamma(\gamma_M - 3\gamma_\sigma) + 2\gamma_\sigma(\gamma_M - \gamma_\sigma)] + 8[8\Gamma^3 + 32\Gamma\gamma_\sigma^2 - 2\gamma_\sigma^2(\gamma_M - 7\gamma_\sigma) + \Gamma^2(\gamma_M + 25\gamma_\sigma)]\Omega_\sigma^2 + 256\Gamma\Omega_\sigma^4\right\}$$
$$\times \left[\gamma_M(\gamma_M - \Gamma)(\gamma_M - \gamma_\sigma)(\gamma_M + \gamma_\sigma)^2(\gamma_M + \gamma_\sigma - 2\Gamma)(\gamma_M + 3\gamma_\sigma - 4\Gamma)(\gamma_M + 3\gamma_\sigma - 2\Gamma)\left(\gamma_{11}\gamma_{21} + 8\Omega_\sigma^2\right)\left(\gamma_{11}^2\gamma_{12} + 8\Gamma\Omega_\sigma^2\right)^2\right]^{-1}, \tag{B1}$$

$$\mathcal{G}_2 \equiv \mathcal{G}_1 \text{ with } \gamma_M \leftrightarrow -\gamma_M, \tag{B2}$$

$$\mathcal{G}_3 \equiv 2\frac{\Gamma\gamma_\sigma\gamma_{11}[\gamma_{1\bar{2}}\gamma_{11}^3\gamma_{21}^2\gamma_{12}^2 + 8\gamma_{11}^2\gamma_{12}\Omega_\sigma^2\left(17\Gamma^3 + 12\Gamma^2\gamma_\sigma + 6\Gamma\gamma_\sigma^2 + 4\gamma_\sigma^3\right) + 256\gamma_{11}^2\Omega_\sigma^4\left(5\Gamma^2 + 6\Gamma\gamma_\sigma + 4\gamma_\sigma^2\right) + 2048\Gamma^2\Omega_\sigma^6]}{\gamma_{12}(\gamma_{11}\gamma_{21} + 8\Omega_\sigma^2)(\gamma_{1\bar{2}}\gamma_{1\bar{1}} + 16\Omega_\sigma^2)(\gamma_{11}^2\gamma_{12} + 8\Gamma\Omega_\sigma^2)^2} \tag{B3}$$

$$\mathcal{G}_4 \equiv 2\frac{2\Gamma^3\left(\gamma_\sigma^2 + 8\Omega_\sigma^2\right)\left(\gamma_{11}\gamma_{12} + 16\Omega_\sigma^2\right)\left(\gamma_{11}^2\gamma_{12}^2\gamma_{31} + 48\Gamma\gamma_{11}^2\Omega_\sigma^2 - 256\gamma_\sigma\Omega_\sigma^4\right)}{\gamma_{1\bar{1}}\gamma_{31}\left(\gamma_M^2 - \gamma_{2\bar{1}}^2\right)\left(\gamma_{11}\gamma_{21} + 8\Omega_\sigma^2\right)\left(\gamma_{11}^2\gamma_{12} + 8\Gamma\Omega_\sigma^2\right)^2}, \tag{B4}$$

$$\mathcal{G}_5 \equiv 2\Big(-1024\Gamma^2\gamma_{11}\Omega_\sigma^4\left\{\gamma_{11}^2\gamma_{12}^2\gamma_{21}\gamma_{31}\gamma_{32}\left[2\Gamma^2(\gamma_M - 3\gamma_\sigma) - \Gamma\gamma_\sigma(\gamma_M + 3\gamma_\sigma) - 2\gamma_\sigma^2(\gamma_M - \gamma_\sigma)\right]\right.$$
$$+ 8\gamma_{11}\gamma_{12}\Omega_\sigma^2[-108\Gamma^6 + \Gamma^5(215\gamma_M - 1203\gamma_\sigma) + 3\Gamma^4\gamma_\sigma(239\gamma_M - 1081\gamma_\sigma) + \Gamma^3\gamma_\sigma^2(1051\gamma_M - 3947\gamma_\sigma)$$
$$+ \Gamma^2\gamma_\sigma^3(803\gamma_M - 2465\gamma_\sigma) + 10\Gamma\gamma_\sigma^4(31\gamma_M - 77\gamma_\sigma) + 48\gamma_\sigma^5(\gamma_M - 2\gamma_\sigma)]$$
$$+ 128\Omega_\sigma^4[6\Gamma^6 + \Gamma^5(131\gamma_M - 227\gamma_\sigma) + \Gamma^4\gamma_\sigma\left(546\gamma_M - 776\gamma_\sigma\right) + \Gamma^3\gamma_\sigma^2(889\gamma_M - 933\gamma_\sigma)$$

$$+ \Gamma^2 \gamma_\sigma^3 (724\gamma_M - 488\gamma_\sigma) + \Gamma \gamma_\sigma^4 (296\gamma_M - 96\gamma_\sigma) + 48\gamma_M \gamma_\sigma^5 \big]$$

$$+ 2048\Omega_\sigma^6 [74\Gamma^4 + 2\Gamma^3(6\gamma_M + 109\gamma_\sigma) + 5\Gamma^2 \gamma_\sigma(3\gamma_M + 61\gamma_\sigma) + 2\Gamma\gamma_\sigma^2(-\gamma_M + 103\gamma_\sigma) - 4\gamma_\sigma^3(\gamma_M - 13\gamma_\sigma)]$$

$$+ 131\,072\,\Gamma\gamma_{21}\Omega_\sigma^8 \big\}\big)$$

$$\times \big[\gamma_{21}\gamma_M(\gamma_M + \Gamma)(\gamma_M - \gamma_\sigma)(\gamma_M + \gamma_\sigma)^2(\gamma_M - \gamma_{2\bar{3}})(\gamma_{11}\gamma_{21} + 8\Omega_\sigma^2)(\gamma_{11}^2\gamma_{12} + 8\Gamma\Omega_\sigma^2)^2(\gamma_{31}\gamma_{32} + 16\Omega_\sigma^2)\big]^{-1}, \quad \text{(B5)}$$

$$\mathcal{G}_6 \equiv \mathcal{G}_5 \text{ with } \gamma_M \leftrightarrow -\gamma_M, \quad \text{(B6)}$$

$$\mathcal{G}_7 \equiv \big\{ 32\Gamma^2 \gamma_{11}(\gamma_\sigma^2 + 8\Omega_\sigma^2)\big[(\gamma_{11}\gamma_{12} + 16\Omega_\sigma^2)(\gamma_{11}\gamma_{12}\gamma_{21}^2\gamma_{31}^2\gamma_{32}\gamma_{1\bar{1}}\gamma_{1\bar{2}}\gamma_{2\bar{1}})$$

$$+ 8\gamma_{31}\Omega_\sigma^2(142\Gamma^7 + 239\Gamma^6\gamma_\sigma - 241\Gamma^5\gamma_\sigma^2 - 677\Gamma^4\gamma_\sigma^3 + 77\Gamma^3\gamma_\sigma^4 + 832\Gamma^2\gamma_\sigma^5 + 580\Gamma\gamma_\sigma^6 + 128\gamma_\sigma^7)$$

$$+ 64\Omega_\sigma^4(219\Gamma^6 + 386\Gamma^5\gamma_\sigma + 565\Gamma^4\gamma_\sigma^2 + 344\Gamma^3\gamma_\sigma^3 - 98\Gamma^2\gamma_\sigma^4 - 208\Gamma\gamma_\sigma^5 - 56\gamma_\sigma^6)$$

$$+ 1024\Omega_\sigma^6(15\Gamma^4 - 11\Gamma^3\gamma_\sigma - 4\Gamma^2\gamma_\sigma^2 - 16\Gamma\gamma_\sigma^3 - 8\gamma_\sigma^4) - 16384\Omega_\sigma^8\gamma_\sigma\gamma_{21}\big]\big\}$$

$$\times \big[\gamma_{21}\gamma_{31}\gamma_{1\bar{1}}(\gamma_M^2 - \gamma_{2\bar{3}}^2)(\gamma_M^2 - \gamma_{4\bar{3}}^2)(\gamma_{11}\gamma_{21} + 8\Omega_\sigma^2)(\gamma_{11}\gamma_{12} + 8\Omega_\sigma^2)(\gamma_{31}\gamma_{32} + 16\Omega_\sigma^2)\big]^{-1}. \quad \text{(B7)}$$

While these expressions are not particularly enlightening, they provide the most general and exact closed-form formula for the filtered coherently driven 2LS. One cannot but marvel at how mathematics introduces unexpected factors to thwart cancellations of these expression so as to ultimately provide what we interpret in physical terms, such as an elbow in a curve, that correspond to the Mollow triplet splitting into three spectral lines.

[1] H. Paul, Photon antibunching, Rev. Mod. Phys. **54**, 1061 (1982).

[2] R. Hanbury Brown and R. Q. Twiss, A test of a new type of stellar interferometer on Sirius, Nature (London) **178**, 1046 (1956).

[3] H. J. Kimble, M. Dagenais, and L. Mandel, Photon Antibunching in Resonance Fluorescence, Phys. Rev. Lett. **39**, 691 (1977).

[4] A. V. Kuhlmann, J. H. Prechtel, J. Houel, A. Ludwig, D. Reuter, A. D. Wieck, and R. J. Warburton, Transform-limited single photons from a single quantum dot, Nat. Commun. **6**, 8204 (2015).

[5] J. C. Gallop, *SQUIDS, the Josephson Effects and Superconducting Electronics* (CRC, Boca Raton, 1990).

[6] L. Schweickert, K. D. Jöns, K. D. Zeuner, S. F. C. da Silva, H. Huang, T. Lettner, M. Reindl, J. Zichi, R. Trotta, A. Rastelli, and V. Zwiller, On-demand generation of background-free single photons from a solid-state source, Appl. Phys. Lett. **112**, 093106 (2018).

[7] L. Hanschke, K. A. Fischer, S. Appel, D. Lukin, J. Wierzbowski, S. Sun, R. Trivedi, J. Vučković, J. J. Finley, and K. Müller, Quantum dot single-photon sources with ultra-low multi-photon probability, npj Quantum Inf. **4**, 43 (2018).

[8] M. Müller, S. Bounouar, K. D. Jöns, M. Glässl, and P. Michler, On-demand generation of indistinguishable polarization-entangled photon pairs, Nat. Photon. **8**, 224 (2014).

[9] Y.-J. Wei, Y.-M. He, M.-C. Chen, Y.-N. Hu, Y. He, D. Wu, C. Schneider, M. Kamp, S. Höfling, C.-Y. Lu, and J.-W. Pan, Deterministic and robust generation of single photons from a single quantum dot with 99.5% indistinguishability using adiabatic rapid passage, Nano Lett. **14**, 6515 (2014).

[10] L. Sapienza, M. Davanço, A. Badolato, and K. Srinivasa, Nanoscale optical positioning of single quantum dots for bright and pure single-photon emission, Nat. Commun. **6**, 7833 (2015).

[11] T. Miyazawa, K. Takemoto, Y. Nambu, S. Miki, T. Yamashita, H. Terai, M. Fujiwara, M. Sasaki, Y. Sakuma, M. Takatsu, T. Yamamoto, and Y. Arakawa, Single-photon emission at 1.5 μm from an InAs/InP quantum dot with highly suppressed multi-photon emission probabilities, Appl. Phys. Lett. **109**, 132106 (2016).

[12] X. Ding, Y. He, Z.-C. Duan, N. Gregersen, M.-C. Chen, S. Unsleber, S. Maier, C. Schneider, M. Kamp, S. Höfling, C.-Y. Lu, and J.-W. Pan, On-Demand Single Photons with High Extraction Efficiency and Near-Unity Indistinguishability from a Resonantly Driven Quantum Dot in a Micropillar, Phys. Rev. Lett. **116**, 020401 (2016).

[13] N. Somaschi, V. Giesz, L. D. Santis, J. C. Loredo, M. P. Almeida, G. Hornecker, S. L. Portalupi, T. Grange, C. Antón, J. Demory, C. Gómez, I. Sagnes, N. D. Lanzillotti-Kimura, A. Lemaître, A. Auffeves, A. G. White, L. Lanco, and P. Senellart, Near-optimal single-photon sources in the solid state, Nat. Photon. **10**, 340 (2016).

[14] S. Unsleber, Y.-M. He, S. Gerhardt, S. Maier, C.-Y. Lu, J.-W. Pan, N. Gregersen, M. Kamp, C. Schneider, and S. Höfling, Highly indistinguishable on-demand resonance fluorescence photons from a deterministic quantum dot micropillar device with 74% extraction efficiency, Opt. Express **24**, 8539 (2016).

[15] H. Wang, Z.-C. Duan, Y.-H. Li, S. Chen, J.-P. Li, Y.-M. He, M.-C. Chen, Y. He, X. Ding, C.-Z. Peng, C. Schneider, M. Kamp, S. Höfling, C.-Y. Lu, and J.-W. Pan, Near-Transform-Limited Single Photons from an Efficient Solid-state Quantum emitter, Phys. Rev. Lett. **116**, 213601 (2016).

[16] D. B. Higginbottom, L. Slodička, G. Araneda, L. Lachman, R. Filip, M. Hennrich, and R. Blatt, Pure single photons from a trapped atom source, New J. Phys. **18**, 093038 (2016).

[17] D. Huber, M. Reindl, Y. Huo, H. Huang, J. S. Wildmann, O. G. Schmidt, A. Rastelli, and R. Trotta, Highly indistinguishable and strongly entangled photons from symmetric GaAs quantum dots, Nat. Commun. **8**, 15506 (2017).

[18] P. Senellart, G. Solomon, and A. White, High-performance semiconductor quantum-dot single-photon sources, Nat. Nanotech. **12**, 1026 (2017).

[19] J. Liu, K. Konthasinghe, M. Davanço, J. Lawall, V. Anant, V. Verma, R. Mirin, S. W. Nam, J. D. Song, B. Ma, Z. S. Chen, H. Q. Ni, Z. C. Niu, and K. Srinivasan, Single Self-Assembled InAs/GaAs Quantum Dots in Photonic Nanostructures: The Role of Nanofabrication, Phys. Rev. Appl. **9**, 064019 (2018).

[20] A. Musiał, P. Holewa, P. Wyborski, M. Syperek, A. Kors, J. P. Reithmaier, G. Sęk, and M. Benyoucef, High-purity triggered single-photon emission from symmetric single InAs/InP quantum dots around the telecom C-band window, Adv. Quantum Technol. **3**, 1900082 (2020).

[21] Y. Arakawa and M. J. Holmes, Progress in quantum-dot single photon sources for quantum information technologies: A broad spectrum overview, Appl. Phys. Rev. **7**, 021309 (2020).

[22] J. C. López Carreño, C. Sánchez Muñoz, E. del Valle, and F. P. Laussy, Excitation with quantum light. II. Exciting a two-level system, Phys. Rev. A **94**, 063826 (2016).

[23] M. C. Teich and B. E. A. Saleh, Photon bunching and antibunching, Prog. Opt. **26**, 1 (1988).

[24] R. J. Glauber, Coherent and incoherent states of the radiation field, Phys. Rev. **131**, 2766 (1963).

[25] L. Mandel and E. Wolf, *Optical Coherence and Quantum Optics* (Cambridge University Press, Cambridge, 1995).

[26] M. O. Scully and M. S. Zubairy, *Quantum Optics* (Cambridge University Press, Cambridge, 2002).

[27] M. C.Teich, B. E. A. Saleh, and D. Stoler, Antibunching in the Franck-Hertz experiment, Opt. Commun. **46**, 244 (2983).

[28] X. T. Zou and L. Mandel, Photon-antibunching and sub-Poissonian photon statistics, Phys. Rev. A **41**, 475 (1990).

[29] P. Michler, A. Kiraz, C. Becher, W. V. Schoenfeld, P. M. Petroff, L. Zhang, E. Hu, and A. Imamoglu, A quantum dot single-photon turnstile device, Science **290**, 2282 (2000).

[30] E. Zubizarreta Casalengua, J. C. López Carreño, E. del Valle, and F. P. Laussy, Structure of the harmonic oscillator in the space of *n*-particle Glauber correlators, J. Math. Phys. **58**, 062109 (2017).

[31] P. Grünwald, Effective second-order correlation function and single-photon detection, New J. Phys. **21**, 093003 (2019).

[32] R. Hanbury Brown, R. C. Jennison, and M. K. D. Gupta, Apparent angular sizes of discrete radio sources: Observations at Jodrell Bank, Manchester, Nature (London) **170**, 1061 (1952).

[33] R. Hanbury Brown and R. Twiss, A new type of interferometer for use in radio astronomy, Philos. Mag. **45**, 663 (1954).

[34] R. Hanbury Brown and R. Q. Twiss, Correlation between photons in two coherent beams of light, Nature (London) **177**, 27 (1956).

[35] E. M. Purcell, The question of correlation between photons in coherent light rays, Nature (London) **178**, 1449 (1956).

[36] D. Stoler, Photon Antibunching and Possible Ways to Observe It, Phys. Rev. Lett. **33**, 1397 (1974).

[37] C. Silberhorn, Detecting quantum light, Contemp. Phys. **48**, 143 (2007).

[38] B. E. Kardynał, Z. L. Yuan, and A. J. Shields, An avalanche-photodiode-based photon-number-resolving detector, Nat. Photon. **2**, 425 (2008).

[39] R. H. Hadfield, Single-photon detectors for optical quantum information applications, Nat. Photon. **3**, 696 (2009).

[40] Z. L. Yuan, B. E. Kardynal, A. W. Sharpe, and A. J. Shields, High speed single photon detection in the near infrared, Appl. Phys. Lett. **91**, 041114 (2007).

[41] J. Wiersig, C. Gies, F. Jahnke, M. Aßmann, T. Berstermann, M. Bayer, C. Kistner, S. Reitzenstein, C. Schneider, S. Höfling, A. Forchel, C. Kruse, J. Kalden, and D. Homme, Direct observation of correlations between individual photon emission events of a microcavity laser, Nature (London) **460**, 245 (2009).

[42] B. Silva, Reaching quantum polaritons, Ph.D. thesis, Universidad Autónoma de Madrid, 2016.

[43] M. Klaas, E. Schlottmann, H. Flayac, F. Laussy, F. Gericke, M. Schmidt, M. Helversen, J. Beyer, S. Brodbeck, H. Suchomel, S. Höfling, S. Reitzenstein, and C. Schneider, Photon-Number-Resolved Measurement of an Exciton-Polariton Condensate, Phys. Rev. Lett. **121**, 047401 (2018).

[44] H.-A. Bachor and T. C. Ralph, *A Guide to Experiments in Quantum Optics* (Wiley, New York, 2004).

[45] S. Reynaud, La fluorescence de résonance: Étude par la méthode de l'atome habillé, Ann. Phys. (Paris) **8**, 315 (1983).

[46] L. Hanschke, L. Schweickert, J. C. López Carreño, E. Schöll, K. D. Zeuner, T. Lettner, E. Zubizarreta Casalengua, M. Reindl, S. F. C. da Silva, R. Trotta, J. J. Finley, A. Rastelli, E. del Valle, F. P. Laussy, V. Zwiller, K. Müller, and K. D. Jöns, Origin of Antibunching in Resonance Fluorescence, Phys. Rev. Lett. **125**, 170402 (2020).

[47] G. S. Agarwal and S. Dutta Gupta, Steady states in cavity QED due to incoherent pumping, Phys. Rev. A **42**, 1737 (1990).

[48] Y. Mu and C. M. Savage, One-atom lasers, Phys. Rev. A **46**, 5944 (1992).

[49] O. Benson and Y. Yamamoto, Master-equation model of a single-quantum-dot microsphere laser, Phys. Rev. A **59**, 4756 (1999).

[50] W. Heitler, *The Quantum Theory of Radiation* (Oxford University Press, Oxford, 1944).

[51] D. Stucki, G. Ribordy, A. Stefanov, H. Zbinden, J. G. Rarity, and T. Wall, Photon counting for quantum key distribution with peltier cooled InGaAs/InP APDs, J. Mod. Opt. **48**, 1967 (2001).

[52] L. Yuan, Z. Yu-Chi, Z. Peng-Fei, G. Yan-Qiang, L. Gang, W. Jun-Min, and Z. Tian-Cai, Experimental study on coherence time of a light field with single photon counting, Chin. Phys. Lett. **26**, 074205 (2009).

[53] M. C. Teich and B. E. A. Saleh, Effects of random deletion and additive noise on bunched and antibunched photon-counting statistics, Opt. Lett. **7**, 365 (1982).

[54] E. Zubizarreta Casalengua, J. C. López Carreño, F. P. Laussy, and E. del Valle, Tuning photon statistics with coherent fields, Phys. Rev. A **101**, 063824 (2020).

[55] J. Eberly and K. Wódkiewicz, The time-dependent physical spectrum of light, J. Opt. Soc. Am. **67**, 1252 (1977).

[56] E. del Valle, A. González-Tudela, F. P. Laussy, C. Tejedor, and M. J. Hartmann, Theory of Frequency-Filtered and Time-Resolved *n*-Photon Correlations, Phys. Rev. Lett. **109**, 183601 (2012).

[57] B. Silva, C. S. Muñoz, D. Ballarini, A. González-Tudela, M. de Giorgi, G. Gigli, K. West, L. Pfeiffer, E. del Valle, D. Sanvitto, and F. P. Laussy, The colored Hanbury Brown–Twiss effect, Sci. Rep. **6**, 37980 (2016).

[58] S. M. Ulrich, C. Gies, S. Ates, J. Wiersig, S. Reitzenstein, C. Hofmann, A. Löffler, A. Forchel, F. Jahnke, and P. Michler, Photon Statistics of Semiconductor Microcavity Lasers, Phys. Rev. Lett. **98**, 043906 (2007).

[59] L. Fleury, J.-M. Segura, G. Zumofen, B. Hecht, and U. P. Wild, Nonclassical Photon Statistics in Single-Molecule Fluorescence at Room Temperature, Phys. Rev. Lett. **84**, 1148 (2000).

[60] C. Kurtsiefer, S. Mayer, P. Zarda, and H. Weinfurter, Stable Solid-State Source of Single Photons, Phys. Rev. Lett. **85**, 290 (2000).

[61] G. Messin, J. P. Karr, A. Baas, G. Khitrova, R. Houdré, R. P. Stanley, U. Oesterle, and E. Giacobino, Parametric Polariton Amplification in Semiconductor Microcavities, Phys. Rev. Lett. **87**, 127403 (2001).

[62] E. B. Flagg, A. Muller, J. W. Robertson, S. Founta, D. G. Deppe, M. Xiao, W. Ma, G. J. Salamo, and C. K. Shih, Resonantly driven coherent oscillations in a solid-state quantum emitter, Nat. Phys. **5**, 203 (2009).

[63] M. Nothaft, S. Höhla, F. Jelezko, N. Frühauf, J. Pflaum, and J. Wrachtrup, Electrically driven photon antibunching from a single molecule at room temperature, Nat. Commun. **3**, 628 (2012).

[64] K. Konthasinghe, J. Walker, M. Peiris, C. K. Shih, Y. Yu, M. F. Li, J. F. He, L. J. Wang, H. Q. Ni, Z. C. Niu, and A. Muller, Coherent versus incoherent light scattering from a quantum dot, Phys. Rev. B **85**, 235315 (2012).

[65] C. Matthiesen, A. N. Vamivakas, and M. Atatüre, Subnatural Linewidth Single Photons from a Quantum Dot, Phys. Rev. Lett. **108**, 093602 (2012).

[66] Y.-M. He, Y. He, Y.-J. Wei, D. Wu, M. Atatüre, C. Schneider, S. Höfling, M. Kamp, C.-Y. Lu, and J.-W. Pan, On-demand semiconductor single-photon source with near-unity indistinguishability, Nat. Nanotech. **8**, 213 (2013).

[67] G. Reithmaier, M. Kaniber, F. Flassig, S. Lichtmannecker, K. Müller, A. Andrejew, J. Vučković, R. Gross, and J. J. Finley, On-chip generation, routing, and detection of resonance fluorescence, Nano Lett. **15**, 5208 (2015).

[68] Y. He, Y.-M. He, J. Liu, Y.-J. Wei, H. Y. Ramírez, M. Atatüre, C. Schneider, M. Kamp, S. Höfling, C.-Y. Lu, and J.-W. Pan, Dynamically Controlled Resonance Fluorescence Spectra From a Doubly Dressed Single InGaAs Quantum Dot, Phys. Rev. Lett. **114**, 097402 (2015).

[69] S. Kumar, M. Brotóns-Gisbert, R. Al-Khuzheyri, A. Branny, G. Ballesteros-Garcia, J. F. Sánchez-Royo, and B. Gerardot, Resonant laser spectroscopy of localized excitons in monolayer WSe₂, Optica **3**, 882 (2016).

[70] R. N. E. Malein, T. S. Santana, J. M. Zajac, A. C. Dada, E. M. Gauger, P. M. Petroff, J. Y. Lim, J. D. Song, and B. D. Gerardot, Screening Nuclear Field Fluctuations in Quantum Dots for Indistinguishable photon generation, Phys. Rev. Lett. **116**, 257401 (2016).

[71] S. Gao, M. Cui, R. Li, L. Liang, Y. Liu, and L. Xie, Quantitative deconvolution of autocorrelations and cross correlations from two-dimensional lifetime decay maps in fluorescence lifetime correlation spectroscopy, Sci. Bull. **62**, 9 (2017).

[72] H. J. Snijders, J. A. Frey, J. Norman, H. Flayac, V. Savona, A. C. Gossard, J. E. Bowers, M. P. van Exter, D. Bouwmeester, and W. Löffler, Observation of the Unconventional Photon Blockade, Phys. Rev. Lett. **121**, 043601 (2018).

[73] S. Zhao, J. Lavie, L. Rondin, L. Orcin-Chaix, C. Diederichs, P. Roussignol, Y. Chassagneux, C. Voisin, K. Müllen, A. Narita, S. Campidelli, and J.-S. Lauret, Single photon emission from graphene quantum dots at room temperature, Nat. Commun. **9**, 3470 (2018).

[74] T. Fink, A. Schade, S. Höfling, C. Schneider, and A. Iˇmamogˇlu, Signatures of a dissipative phase transition in photon correlation measurements, Nat. Phys. **14**, 365 (2018).

[75] F. Liu, A. J. Brash, J. O'Hara, L. M. P. Martins, C. Phillips, R. J. Cole., B. Royall, E. Clarke, C. Bentham, N. Prtljaga, I. E. Itskevich, L. R. Wilson, M. S. Skolnick, and M. A. Fox, High Purcell factor generation of indistinguishable on-chip single photons, Nat. Nanotech. **13**, 835 (2018).

[76] A. P. Foster, D. Hallett, I. V. Iorsh, S. J. Sheldon, M. R. Godsland, B. Royall, E. Clarke, I. A. Shelykh, A. M. Fox, M. S. Skolnick, I. E. Itskevich, and L. R. Wilson, Tunable Photon Statistics Exploiting the Fano Effect in a Waveguide, Phys. Rev. Lett. **122**, 173603 (2019).

[77] J. Liu, R. Su, Y. Wei, B. Yao, S. F. C. da Silva, Y. Yu, J. Iles-Smith, K. Srinivasan, A. Rastelli, J. Li, and X. Wang, A solid-state source of strongly entangled photon pairs with high brightness and indistinguishability, Nat. Nanotech. **14**, 586 (2019).

[78] M. Anderson, T. Müller, J. Huwer, J. Skiba-Szymanska, A. B. Krysa, R. M. Stevenson, J. H. D. A., Ritchie, and A. J. Shields, Quantum teleportation using highly coherent emission from telecom C-band quantum dots, npj Quantum Inf. **6**, 14 (2020).

[79] C. L. Phillips, A. J. Brash, D. P. S. McCutcheon, J. Iles-Smith, E. Clarke, B. Royall, M. S. Skolnick, and A. M. Fox, and A. Nazir, Photon Statistics of Filtered Resonance Fluorescence, Phys. Rev. Lett. **125**, 043603 (2020).

[80] C. Cohen-Tannoudji and S. Reynaud, Atoms in strong light-fields: Photon antibunching in single atom fluorescence, Philos. Trans. R. Soc. London Ser. A **293**, 223 (1979).

[81] J. Dalibard and S. Reynaud, Correlation signals in resonance fluorescence: Interpretation via photon scattering amplitudes, J. Phys. (Paris) **44**, 1337 (1983).

[82] H. F. Arnoldus and G. Nienhuis, Photon correlations between the lines in the spectrum of resonance fluorescence, J. Phys. B **17**, 963 (1984).

[83] H. F. Arnoldus and G. Nienhuis, Atomic fluorescence in a mode-hopping laser field, J. Phys. B **19**, 2421 (1986).

[84] G. Nienhuis, Spectral correlations in resonance fluorescence, Phys. Rev. A **47**, 510 (1993).

[85] K. Joosten and G. Nienhuis, Influence of spectral filtering on the quantum nature of light, J. Phys. B **2**, 158 (2000).

[86] C. W. Gardiner, Driving a Quantum System with the Output Field from Another Driven Quantum System, Phys. Rev. Lett. **70**, 2269 (1993).

[87] H. Carmichael, *An Open Systems Approach to Quantum Optics* (Springer, Berlin, 1993), Chap. 6, p. 110.

[88] J. C. López Carreño, E. del Valle, and F. P. Laussy, Frequency-resolved Monte Carlo, Sci. Rep. **8**, 6975 (2018).

[89] K. Kamide, S. Iwamoto, and Y. Arakawa, Eigenvalue decomposition method for photon statistics of frequency-filtered fields and its application to quantum dot emitters, Phys. Rev. A **92**, 033833 (2015).

[90] R. Centeno Neelen, D. M. Boersma, M. P. van Exter, G. Nienhuis, and J. P. Woerdman, Spectral Filtering within the

Schawlow-Townes Linewidth of a Semiconductor Laser, Phys. Rev. Lett. **69**, 593 (1992).

[91] A. González-Tudela, F. P. Laussy, C. Tejedor, M. J. Hartmann, and E. del Valle, Two-photon spectra of quantum emitters, New J. Phys. **15**, 033036 (2013).

[92] J. C. López Carreño and F. P. Laussy, Excitation with quantum light. I. Exciting a harmonic oscillator, Phys. Rev. A **94**, 063825 (2016).

[93] C. Sánchez Muñoz, E. del Valle, A. G. Tudela, K. Müller, S. Lichtmannecker, M. Kaniber, C. Tejedor, J. Finley, and F. Laussy, Emitters of *N*-photon bundles, Nat. Photon. **8**, 550 (2014).

[94] M. N. Makhonin, J. E. Dixon, R. J. Coles, B. Royall, I. J. Luxmoore, E. Clarke, M. Hugues, M. S. Skolnick, and A. M. Fox, Waveguide coupled resonance fluorescence from on-chip quantum emitter, Nano Lett. **14**, 6997 (2014).

[95] M. Peiris, B. Petrak, K. Konthasinghe, Y. Yu, Z. C. Niu, and A. Muller, Two-color photon correlations of the light scattered by a quantum dot, Phys. Rev. B **91**, 195125 (2015).

[96] Y. Nieves and A. Muller, Third-order frequency-resolved photon correlations in resonance fluorescence, Phys. Rev. B **98**, 165432 (2018).

[97] J. C. López Carreño, E. del Valle, and F. P. Laussy, Photon correlations from the Mollow triplet, Laser Photon. Rev. **11**, 1700090 (2017).

[98] E. Zubizarreta Casalengua, J. C. López Carreño, F. P. Laussy, and E. del Valle, Conventional and unconventional photon statistics, Laser Photon. Rev. **14**, 1900279 (2020).

[99] C. A. Schrama, G. Nienhuis, H. A. Dijkerman, C. Steijsiger, and H. G. M. Heideman, Intensity correlations between the components of the resonance fluorescence triplet, Phys. Rev. A **45**, 8045 (1992).

[100] I. V. Panyukov, V. Y. Shishkov, and E. S. Andrianov, Second-order autocorrelation function of spectrally filtered light from an incoherently pumped two-level system, Ann. Phys. **534**, 2100286 (2022)